Zhang, Tingting; Vorobyov, Sergiy A.; Xu, Feng

Transmit Energy Focusing for Parameter Estimation in Slow-time Transmit Beamspace L-shaped MIMO Radar

Published in:
IEEE Transactions on Signal Processing

DOI:
10.1109/TSP.2024.3492692

Published: 06/11/2024

Document Version
Publisher's PDF, also known as Version of record

Transmit Energy Focusing for Parameter Estimation in Slow-Time Transmit Beamspace L-Shaped MIMO Radar

Tingting Zhang, *Student Member, IEEE*, Sergiy A. Vorobyov, *Fellow, IEEE*, and Feng Xu, *Member, IEEE*

***Abstract*—We present a novel slow-time transmit beamspace (TB) multiple-input multiple-output (MIMO) technique for L-shaped array radar with uniform linear subarrays to estimate target parameters including 2-dimensional (2-D) directions of arrival (DOA) and unambiguous velocity. Doppler division multiple access (DDMA) approach, as a type of slow-time waveform achieving waveform orthogonality across multiple pulses within a coherent processing interval, disperses the transmit energy over the entire spatial region, suffering from beam-shape loss. Moreover, Doppler spectrum division, which is necessary for transmit channel separation prior to parameter estimation, leads to the loss of crucial information for velocity disambiguation. To optimize transmit energy distribution, slow-time TB technique is proposed to focus the energy within a desired spatial region. Unlike DDMA approach, slow-time TB technique divides the entire Doppler spectrum into more subbands than the number of transmit antenna elements to narrow down the beam mainlobe intervals between adjacent beams formed by DDMA modulation vectors. As a result, more beams are incorporated into the region of interest, and slow-time TB radar can direct transmit energy to the region of interest by properly selecting the DDMA modulation vectors whose beams are directed there. To resolve velocity ambiguity, tensor signal modeling, by storing measurements in a tensor without Doppler spectrum division, is used. Parameter estimation is then addressed using canonical polyadic decomposition (CPD), and the performance of slow-time TB L-shaped MIMO radar is shown to be improved as compared to DDMA MIMO techniques. Simulations are conducted to validate the proposed method.**

***Index Terms*—Slow-time transmit beamspace, 2-D DOA estimation, CPD, L-shaped array, velocity disambiguation.**

I. Introduction

In the last two decades, multiple-input multiple-output (MIMO) radars [1], [2], [3], [4], [5] have received a great deal of attention and seen prosperous development. More degrees of freedom and a larger virtual radar aperture, which amount to more detectable targets with higher spatial resolution, can be achieved by the transmission of multiple independent waveforms from different transmit channels, which is what differentiates MIMO radars from phased-array radars [6], [7]. To ensure the benefits listed above, waveform diversity is one of the research focuses in the MIMO radar field.

Waveforms of various types, including frequency division multiple access (FDMA) [8], code division multiple access (CDMA) [9], time division multiple access (TDMA) [10], and Doppler division multiple access (DDMA) [9], [11], have been developed. Among them, TDMA stood out due to its easy implementation and low hardware cost. The most basic and intuitive way to achieve orthogonality between transmit channels is to alternately activate transmit antenna elements without overlapping, which is exactly the core concept of TDMA. However, TDMA's transmission capability is seriously underutilized and its average transmit power is significantly lower when compared to other waveforms whose transmit antennas radiate signals simultaneously, resulting in a reduced detectable range.

More transmit antennas will be required in pursuit of higher system performance in the future, further reducing the average transmit power of TDMA. Meanwhile, a higher pulse repetition frequency (PRF) is required to avoid Doppler ambiguity in the presence of high-speed vehicles, whereas range ambiguity arises as a result of the higher PRF. TDMA exacerbates this conflict because of its alternate transmission. Given the foregoing, TDMA is no longer as appealing as it once was, and DDMA technique is capturing the research attention. DDMA technique, inheriting the TDMA's transmitter configuration, achieves waveform diversity in the slow time [8], [12] by modulating each transmit channel with a different Doppler shift. For DDMA technique, transmission capability is fully utilized, and transmit channel divisibility is accomplished as well.

Estimating 2-dimensional (2-D) directions of arrival (DOA), including azimuth and elevation angles, is a topic of considerable interest for real-world applications. Among these applications, radar systems for detection and localization are

Received 8 November 2023; revised 26 July 2024 and 28 October 2024; accepted 2 November 2024. Date of publication 6 November 2024; date of current version 18 November 2024. This work was supported in part by the Academy of Finland under Grant 357715. The associate editor coordinating the review of this article and approving it for publication was Dr. Emanuele Grossi. *(Corresponding author: Sergiy A. Vorobyov.)*

Tingting Zhang and Sergiy A. Vorobyov are with the Department of Information and Communications Engineering, Aalto University, 02150 Espoo, Finland (e-mail: tingting.zhang@aalto.fi; svor@ieee.org).

Feng Xu is with the Department of Information and Communications Engineering, Aalto University, 02150 Espoo, Finland, and also with Nokia, 02610 Espoo, Finland (e-mail: feng.xu@aalto.fi).

Digital Object Identifier 10.1109/TSP.2024.3492692

integral components of modern advanced driver assistance systems and autonomous vehicles, aimed at reducing human error and enhancing vehicle safety [13], [14]. To achieve reliable functionality, the performance of 2-D DOA estimation is crucial for automotive radar systems. Several 2-D array structures such as uniform rectangular array (URA), circular array, and L-shaped array have been intensively employed. Although all of these array structures find their applications in practice, the L-shaped array has been found to be superior to URA due to a significantly lower (37%) Carmér-Rao bound (CRB) on DOA estimation [15]. Moreover, L-shaped arrays are easy to implement in comparison to some other array structures among 2-D planar arrays for 2-D DOA estimation that have been developed, leading to L-shaped arrays being at the forefront of array processing research [15], [16], [17], [18], [19], [20], [21], [22].

This paper considers an L-shaped array with two subarrays shaped as uniform linear arrays (ULAs) positioned along the x-axis and z-axis, respectively, where azimuth and elevation angles can be estimated by processing the signals transmitted from subarrays along the x-axis and z-axis separately. In other words, 2-D DOA estimation can be converted into 1-dimensional (1-D) angle estimation with a two-fold operation. Thus, the majority of 1-D DOA estimation algorithms can be used in L-shaped arrays with few adaptations. Considering the benefits of both the DDMA waveform and the L-shaped array configuration, DDMA technique is proposed for L-shaped array MIMO radar. Even though the entire Doppler spectrum can be uniformly divided into the number of transmit elements of two subarrays to achieve channel separation among all the transmit channels of an L-shaped array, the number of pulse samples will inevitably be reduced as many times as the number of total transmit elements. As a result, parameter estimation performance deteriorates, particularly at a low signal-to-noise ratio (SNR). As a compromise, additional two waveforms orthogonal in the fast time are used. As a result, independence between subarrays is realized in the fast time, while waveform diversity within subarray elements is achieved in the slow time, e.g., DDMA.

Existing 2-D DOA estimation algorithms range from adoption of nonparametric Fourier-based methods [23] and traditional beamforming techniques such as Capon beamformer to higher-resolution parametric methods like multiple signal classification (MUSIC) [24], [25] and estimation of signal parameters via rotational invariance technique (ESPRIT) [26]. However, these algorithms work with the multidimensional received measurements collected into a matrix form. As a consequence, the multi-linear structure inherent in the signal is not exploited. It has been validated that tensor-based methods outperform matrix-based methods, especially in low SNR cases [27], [28], [29], [30]. Therefore, tensor representation has been used for DOA estimation. Existing tensor-based methods can be mainly categorized into higher order singular value decomposition [29], [31], canonical polyadic decomposition (CPD), also named as parallel factor (PARAFAC) analysis [32], [33], constrained tensor decomposition [34], [35], and more recently learning-based techniques [36], [37]. The first two classes of methods are applicable for tensors with arbitrary factors, whereas the third one is intended for tensors with factor matrices that obey a certain structure, for example, Vandermonde structure. The methods from the last class help to significantly reduce the computational complexity at the testing phase, and show more efficiency also when the known tensor structure is exploited.

To apply tensor representation to DDMA MIMO radar, [38] has proposed a tensor model and developed a modified alternating least squares (ALS) tensor decomposition algorithm for DOA estimation. However, Doppler spectrum division, which inevitably downsamples the pulse data and leads to the loss of velocity information that originally was present between adjacent pulses, is still demanded for transmit channel separation in [38]. As a result, the unambiguous velocity is reduced as many times as the number of transmit elements, and velocity ambiguity tends to arise for high-speed targets. To address this issue, a method called PARAFAC-Direct in [39] designs a tensor model for DDMA radar measurements, obviating the requirement for Doppler spectrum division. Thus, velocity information is well preserved, and unambiguous velocity can be restored.

Although MIMO radar gains more degrees of freedom and a larger virtual aperture thanks to waveform diversity compared to phased-array radar, its transmit energy is distributed omnidirectionally, resulting in transmit energy waste and lower SNRs. It is acknowledged that a higher SNR contributes to better radar system performance [2]. Hence, coherent transmit beamspace (TB) design techniques have been developed in [7], [28], [35], [40] in the last decade to improve parameter estimation performance even further. With prior knowledge of the desired spatial region, transmit beams of orthogonal waveforms can be designed to direct energy toward the desired region, and transmit energy distribution can be optimized.

In this paper, slow-time TB L-shaped MIMO technique is proposed to improve parameter estimation performance.[1] Slow-time MIMO radar, as its name suggests, is a waveform technique that achieves orthogonality in the slow time rather than the fast time, with DDMA technique being a typical example. For traditional DDMA MIMO radar [9], [39], the number of pulses within a pulse cycle equals the number of transmit antenna elements, and each pulse within a cycle is modulated with a different vector. These vectors form distinct beams from one another, and mainlobes of these beams are directed across the entire spatial region. That is to say, transmit energy can be regarded as being distributed over the entire region rather than being focused within a specific limited region of interest. For DDMA technique, the intervals of adjacent beam mainlobes shaped by DDMA modulation vectors for pulses are correlated to the number of transmit elements. The more transmit elements, the closer the adjacent beams get. Therefore, if the entire Doppler spectrum is uniformly divided into more subbands than the number of transmit elements, a larger number of different beams can be formed, and adjacent beam mainlobes get closer

[1]We have recently reported some preliminary concept verification type of results only in [41].

[42]. Consequently, more beams are comprised within a specific sector. With prior knowledge of 2-D spatial sector of interest, those pulses whose beamforming vectors direct their beams toward the desired region are selected for each subarray, and the corresponding phase modulation vectors for those pulses constitute new phase modulation matrices for the proposed slow-time TB MIMO radar. As a result, the transmit energy is successfully focused within the desired region. The novel contributions of this paper can be summarized as follows.

- **Optimization of transmit energy distribution:** Inheriting DDMA's advantages, we propose the slow-time TB L-shaped MIMO radar technique which achieves transmit energy distribution optimization. The latter fact contributes to the performance improvement of the introduced radar system, especially at low SNRs.
- **Enhancing parameter estimation using tensor-based signal model:** A new tensor-based (instead of matrix-based) signal model without Doppler spectrum division is developed in slow-time TB L-shaped MIMO radar for parameter estimation. It preserves the multi-linear structure inherent in the signal measurements to further improve the parameter estimation performance. It resolves the velocity ambiguity as well.
- **Benchmarking against existing algorithms:** The performance of the proposed slow-time TB L-shaped MIMO technique is demonstrated and validated through simulation experiments, benchmarking it against existing parameter estimation algorithms including ESPRIT, CPD, and PARAFAC-Direct. The SNR threshold [40] for the resolution of closely spaced targets, for example, is demonstrated to be approximately 10–15 dB lower than that of the aforementioned algorithms, highlighting the superior efficacy of the proposed approach.

The rest of the paper is organized as follows. In Section II, signal models of DDMA MIMO radar with transmit 1-D ULA and 2-D L-shaped array are introduced. In Section III, the proposed slow-time TB L-shaped array radar is presented. In Section IV, parameter estimation using CPD for L-shaped array radar is developed. Simulation based experiments in Section V validate the effectiveness of the proposed method for energy distribution optimization and parameter estimation, and the conclusion is given in Section VI.

II. Signal Model

A. DDMA MIMO Radar With Transmit ULA

Consider a mono-static pulsed MIMO radar with M_{t} transmit antennas and M_{r} receive antennas.[2] The transmit and receive arrays are assumed to be close enough to each other so that a far-field target can be observed from the same spatial angle by both arrays. Altogether Q pulses are emitted with pulse repetition interval $T_{\mathrm{r}} = 1/\mathrm{PRF}$ within a single coherent processing interval (CPI), and the duration of each pulse is T_{p}. Transmit antenna elements are arranged in the shape of a ULA where the distance between adjacent elements is d_{t}. As a transmit array, d_{t} should be no larger than half a wavelength λ to meet the Nyquist sampling criterion.

Omnidirectional antennas theoretically have the ability to provide 360-degree coverage. However, typically in practice, we first roughly specify the potential spatial area where targets are located, termed the region of interest $\boldsymbol{\Theta}$ in this paper. With $\boldsymbol{\Theta}$ known a *priori*, advanced techniques can be applied to achieve higher accuracy of detection and location. Assuming that there are K targets within the region of interest $\boldsymbol{\Theta}$ with directions[3] θ_k, ranges R_k, and velocities v_k, $k = 1, 2, \ldots, K$, the steering vector of the transmit ULA for the kth target can be expressed as

$$\mathbf{a}(\theta_k) = \left[1, e^{-j2\pi \frac{d_{\mathrm{t}}}{\lambda} \cos\theta_k}, \ldots, e^{-j2\pi \frac{d_{\mathrm{t}}}{\lambda}(M_{\mathrm{t}}-1)\cos\theta_k}\right]^T \quad (1)$$

where $(\cdot)^T$ stands for the transpose operation. Since this work focuses on the transmit energy distribution optimization, we leave the shape of the receive array flexible, and we use $\mathbf{b}(\theta_k)$ to denote the receive steering vector in general.

To achieve waveform orthogonality, with a predesigned phase modulation matrix $\mathbf{W}$ of size $M_{\mathrm{t}} \times Q$, DDMA MIMO radar modulates each transmit channel with a different Doppler shift to achieve the divisibility of transmit signals in the slow time (Doppler) domain. Dividing the whole Doppler frequency spectrum uniformly into M_{t} subbands, the Doppler shift for the mth transmit channel is given as

$$f_m = (m-1)\frac{\mathrm{PRF}}{M_{\mathrm{t}}}, m = 1, 2, \ldots, M_{\mathrm{t}}. \quad (2)$$

For the qth pulse, its phase modulation vector $\mathbf{w}_q$, which is also the qth column of $\mathbf{W}$, can be written as

$$\mathbf{w}_q = \left[1, e^{-j2\pi \frac{\mathrm{PRF}}{M_{\mathrm{t}}}(q-1)T_{\mathrm{r}}}, \ldots, e^{-j2\pi(M_{\mathrm{t}}-1)\frac{\mathrm{PRF}}{M_{\mathrm{t}}}(q-1)T_{\mathrm{r}}}\right]^T, \quad q = 1, 2, \ldots, Q. \quad (3)$$

With DDMA modulation, only a Doppler spectrum subband of width $\mathrm{PRF}/M_{\mathrm{t}}$ is available for each transmit channel. Consequently, the maximum unambiguous velocity is

$$v_{\max} = \frac{\mathrm{PRF}\lambda}{4M_{\mathrm{t}}}. \quad (4)$$

It can be seen from (4) that $v_{\max}$ is reduced by a factor of M_{t} compared to, for example, the case of FDMA where each transmit channel is accessible to the whole Doppler spectrum, which exacerbates the velocity (Doppler) ambiguity.

We assume that the target reflection coefficient obeys Swerling I model [43]. With modulation matrix $\mathbf{W}$ depicted in (3), the received signal by the nth receive antenna element for the qth pulse can be expressed as

$$y_{nq}(t) = \sum_{k=1}^{K}\sum_{m=1}^{M_{\mathrm{t}}} \sigma_k w_{mq} s(t - \tau_{mnq,k}) + z_{nq}(t), \quad n = 1, 2, \ldots, M_{\mathrm{r}} \quad (5)$$

[2] All antennas are assumed to be omnidirectional in this paper.

[3] To be consistent with the subsequent expressions of L-shaped array, θ_k, the complementary angle of the target incident angle, is used instead.

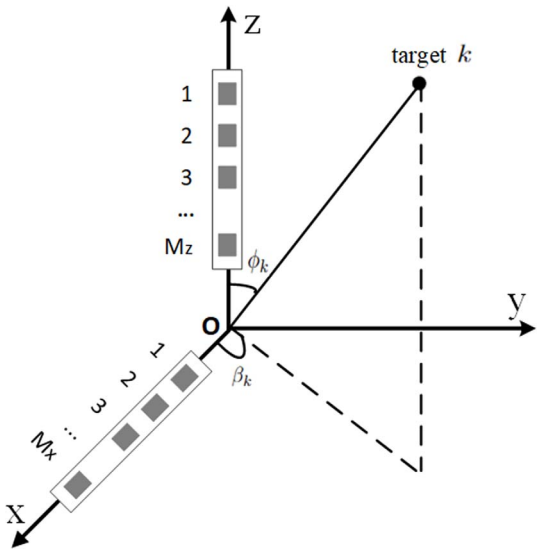

Fig. 1. L-shaped array configuration.

where t is the fast-time index, σ_k is the complex-valued reflection coefficient of the kth target, w_{mq} is the (m,q)-th element of $\mathbf{W}$, $s(t)$ is the transmitted waveform, and $z_{nq}(t)$ is the noise component in the nth receive antenna element for the qth pulse. The time delay $\tau_{mnq,k}$, caused by the wave traveling distance from the mth transmit element to the kth target and then back to the nth receive element for the qth pulse, can be expressed as

$$\tau_{mnq,k} = \frac{2\left(R_k - (q-1)T_{\mathrm{r}}v_k\right) + (m-1)d_{\mathrm{t}}\cos\theta_k + d_{n,k}}{c} \tag{6}$$

where $d_{n,k}$ is the difference in traveling distance from the kth target to the nth element compared to the reference element within the receive array, and c is the light speed. After carrier frequency downconversion and matched filtering, the received signal in (5) can be rewritten as

$$y_{nq} = \sum_{k=1}^{K} \sigma_k e^{j2\pi f_k (q-1)T_{\mathrm{r}}} \left(\mathbf{a}^T(\theta_k)\mathbf{w}_q\right) b_n(\theta_k) + z_{nq} \tag{7}$$

where factor σ_k incorporates other constant factors, $f_k = 2v_k/\lambda$ is the Doppler shift caused by target velocity, $b_n(\theta_k)$ is the nth element of $\mathbf{b}(\theta_k)$, and z_{nq} is the residual noise after filtering.

B. DDMA MIMO Radar With Transmit L-Shaped Array

Extending the 1-D ULA array to a 2-D array for 2-D DOA estimation (azimuth and elevation angles), consider an L-shaped array with two ULAs positioned along the x-axis and z-axis, respectively, as shown in Fig. 1. To distinguish from 1-D array, each ULA within an L-shaped array is referred to as subarray in this paper. Subarrays along the x-axis and z-axis consist of M_{x} and M_{z} antenna elements spaced at distances d_{x} and d_{z} from each other, respectively. The space Cartesian coordinate of the m_{x}th and m_{z}th array elements within the x-axis and z-axis subarrays can be denoted as, respectively,

$$\mathbf{r}_{\mathrm{x},m_{\mathrm{x}}} = ((m_{\mathrm{x}}-1)d_{\mathrm{x}}, 0, 0)^T, m_{\mathrm{x}} = 1, 2, \ldots, M_{\mathrm{x}}$$

$$\mathbf{r}_{\mathrm{z},m_{\mathrm{z}}} = (0, 0, (m_{\mathrm{z}}-1)d_{\mathrm{z}})^T, m_{\mathrm{z}} = 1, 2, \ldots, M_{\mathrm{z}}. \tag{8}$$

In addition, array coordinate matrices $\mathbf{R}_{\mathrm{x}} \in \mathbb{R}^{M_{\mathrm{x}}\times 3}$ and $\mathbf{R}_{\mathrm{z}} \in \mathbb{R}^{M_{\mathrm{z}}\times 3}$ are defined as follows

$$\begin{aligned}\mathbf{R}_{\mathrm{x}} &\triangleq \left[\mathbf{r}_{\mathrm{x},1}, \mathbf{r}_{\mathrm{x},2}, \ldots, \mathbf{r}_{\mathrm{x},M_{\mathrm{x}}}\right]^T \\ \mathbf{R}_{\mathrm{z}} &\triangleq \left[\mathbf{r}_{\mathrm{z},1}, \mathbf{r}_{\mathrm{z},2}, \ldots, \mathbf{r}_{\mathrm{z},M_{\mathrm{z}}}\right]^T.\end{aligned} \tag{9}$$

The 2-D DOAs of the kth far-field target include azimuth angle β_k and elevation angle ϕ_k. Different from the 1-D ULA described in Section II-A, the problem of interest becomes, in this case, the estimation of the DOA pairs $\{\beta_k, \phi_k\}_{k=1}^K$.

Define the propagation vector as

$$\mathbf{p}_k = \left[\sin\phi_k \cos\beta_k, \sin\phi_k \sin\beta_k, \cos\phi_k\right]^T. \tag{10}$$

With $\cos\varphi_k = \sin\phi_k\cos\beta_k$, the transmit steering vectors of two subarrays can be expressed as

$$\begin{aligned}\mathbf{a}_{\mathrm{x}}(\varphi_k) &= e^{-j2\pi\mathbf{R}_{\mathrm{x}}\mathbf{p}_k} \\ &= \left[1, e^{-j2\pi\frac{d_{\mathrm{x}}}{\lambda}\cos\varphi_k}, \ldots, e^{-j2\pi(M_{\mathrm{x}}-1)\frac{d_{\mathrm{x}}}{\lambda}\cos\varphi_k}\right]^T \\ \mathbf{a}_{\mathrm{z}}(\phi_k) &= e^{-j2\pi\mathbf{R}_{\mathrm{z}}\mathbf{p}_k} \\ &= \left[1, e^{-j2\pi\frac{d_{\mathrm{z}}}{\lambda}\cos\phi_k}, \cdots, e^{-j2\pi(M_{\mathrm{z}}-1)\frac{d_{\mathrm{z}}}{\lambda}\cos\phi_k}\right]^T.\end{aligned} \tag{11}$$

Unless otherwise specified, azimuth angle refers to φ_k for convenience from now on. Observing (11), it can be found that azimuth φ_k and elevation ϕ_k are independently contained in two transmit subarrays without coupling, which means that 2-D DOAs can be estimated just by applying existing DOA estimation algorithms to the signals transmitted by the two subarrays separately.

With the orthogonality between two waveforms transmitted by subarrays, a 2-D L-shaped array can be approximately regarded as a combination of two independent ULAs. On this basis, DDMA is applicable to L-shaped array as well except that two DDMA modulation matrices are demanded. To apply the DDMA approach, two phase modulation matrices $\mathbf{W}_{\mathrm{x}}$ and $\mathbf{W}_{\mathrm{z}}$ are designed to modulate transmit channels with different Doppler shifts for each independent subarray. Owing to the independence, $\mathbf{W}_{\mathrm{x}}$ and $\mathbf{W}_{\mathrm{z}}$ can be designed separately based on the practical requirements, which will be covered in depth in Section III. With two orthogonal waveforms $\mathrm{u}_1(t)$ and $\mathrm{u}_2(t)$, the signals transmitted from $M_{\mathrm{x}} + M_{\mathrm{z}}$ antenna elements can be expressed as

$$\mathbf{h}_q(t) = \begin{bmatrix}\mathbf{h}_{\mathrm{x},q}(t) \\ \mathbf{h}_{\mathrm{z},q}(t)\end{bmatrix} = \begin{bmatrix}\mathbf{w}_{\mathrm{x},q}\mathrm{u}_1(t) \\ \mathbf{w}_{\mathrm{z},q}\mathrm{u}_2(t)\end{bmatrix} \tag{12}$$

where $\mathbf{h}_{\mathrm{x},q}(t)$ and $\mathbf{h}_{\mathrm{z},q}(t)$ are the transmitted signals from subarrays along the x-axis and z-axis, and $\mathbf{w}_{\mathrm{x},q}$ and $\mathbf{w}_{\mathrm{z},q}$ are the qth column vectors of $\mathbf{W}_{\mathrm{x}}$ and $\mathbf{W}_{\mathrm{z}}$ for the qth pulse modulation, respectively.

To separate the signals from different subarrays, range compression is performed twice on the received signals with reference signals $\mathrm{u}_i(t), i = 1, 2$, then the separated signals from

two transmit subarrays to the nth receive element can be expressed as

$$\begin{aligned} &y_{\mathrm{x},nq} \\ &\quad=\sum_{k=1}^{K}\sigma_k e^{j2\pi f_k(q-1)T_{\mathrm{r}}}\left(\mathbf{a}_{\mathrm{x}}^{T}\left(\varphi_k\right)\mathbf{w}_{\mathrm{x},q}\right)b_n\left(\varphi_k,\phi_k\right)+z_{\mathrm{x},nq} \\ &y_{\mathrm{z},nq} \\ &\quad=\sum_{k=1}^{K}\sigma_k e^{j2\pi f_k(q-1)T_{\mathrm{r}}}\left(\mathbf{a}_{\mathrm{z}}^{T}\left(\phi_k\right)\mathbf{w}_{\mathrm{z},q}\right)b_n\left(\varphi_k,\phi_k\right)+z_{\mathrm{z},nq} \end{aligned} \tag{13}$$

where $b_n(\varphi_k,\phi_k)$ denotes the nth element of the receive steering vector $\mathbf{b}(\varphi_k,\phi_k)$, and $z_{\mathrm{x},nq}$ and $z_{\mathrm{z},nq}$ are the noise components after range compression. After obtaining the signals from two subarrays as is depicted in (13), parameter estimation algorithms for DDMA MIMO radars can be applied to each subarray, respectively, and thus, target azimuth angles $\{\varphi_k\}_{k=1}^{K}$, elevation angles $\{\phi_k\}_{k=1}^{K}$, and velocities $\{v_k\}_{k=1}^{K}$ can be estimated.

III. Proposed Slow-Time Transmit Beamspace L-Shaped Array Radar

A. Slow-Time Transmit Beamspace Design

Recalling (7), the transmit energy beampattern of DDMA MIMO radar for the qth pulse can be expressed as

$$G(\theta)=\left|\mathbf{a}^{T}\left(\theta\right)\mathbf{w}_q\right|^2 \tag{14}$$

where θ denotes the spatial angle of a target, $|\cdot|$ denotes the element-wise modulus operation on a number or a vector (here a number). It is noteworthy to mention that 1-D ULA and 2-D L-shaped array share the similar property of transmit beamspace, and thus, here the former one is taken as an example to discuss for the ease of description. It can be found from (14) that the energy beampattern for a fixed transmit array configuration depends on the design of DDMA modulation matrix $\mathbf{W}$ consisting of phase modulation vectors $\mathbf{w}_q, q=1,2,\ldots,Q$.

Rewrite the vector $\mathbf{w}_q$ defined in (3) as

$$\mathbf{w}_q=\left[1,e^{-j2\pi\frac{q-1}{M_{\mathrm{t}}}},\ldots,e^{-j2\pi\frac{(M_{\mathrm{t}}-1)(q-1)}{M_{\mathrm{t}}}}\right]^{T}. \tag{15}$$

Observing the ULA steering vector $\mathbf{a}\left(\theta\right)$ in (1), $\mathbf{w}_q$ can be regarded as a beamforming vector with mainlobe direction $\theta_{\mathrm{b},q}$. Taking $d_{\mathrm{t}}=\lambda/2$ as an illustration, which is commonly used in practical radar applications, the mainlobe direction $\theta_{\mathrm{b},q}$ for the qth pulse satisfies

$$\cos\theta_{\mathrm{b},q}=2l-\frac{2(q-1)}{M_{\mathrm{t}}}, q=1,2,\ldots,Q \tag{16}$$

where l is a nonnegative integer just to guarantee that $\cos\theta_{\mathrm{b},q}\in[-1,1]$. It can be found that $\theta_{\mathrm{b},q}$ varies from pulse to pulse with a cycle of M_{t} pulses, and mainlobes of the formed beams in a pulse period sweep across the entire spatial region with specific intervals. As a result, the overall transmit energy within a pulse period is distributed across the whole spatial region rather than focused within a certain spatial sector. If the transmit energy can be focused within the region of interest $\mathbf{\Theta}$, the performance of parameter estimation for targets in this region can be significantly improved due to a higher SNR. In this paper, therefore, a slow-time TB MIMO radar is proposed to optimize the transmit energy distribution and improve the performance of parameter estimation.

Observing (16), we can find that the mainlobe distance between adjacent pulse beams depends on the value of M_{t}, which is also the number of divided subbands in the Doppler domain for traditional DDMA. To distinguish the number of subbands and the number of transmit elements, we use M_{v} to denote the total number of divided subbands, which is also referred to as the number of virtual transmit elements [42]. Meanwhile, the pulse period of modulation vectors becomes M_{v} instead of M_{t}. The Doppler shifts and phase modulation vectors can then be rewritten as

$$f_m=(m-1)\frac{\mathrm{PRF}}{M_{\mathrm{v}}}, m=1,2,\ldots,M_{\mathrm{v}} \tag{17}$$

$$\mathbf{w}_q=\left[1,e^{-j2\pi\frac{q-1}{M_{\mathrm{v}}}},\ldots,e^{-j2\pi\frac{(M_{\mathrm{v}}-1)(q-1)}{M_{\mathrm{v}}}}\right]^{T}, \quad q=1,2,\ldots,Q. \tag{18}$$

With a larger M_{v} than M_{t}, M_{v} Doppler shifts for phase modulation are available for transmit elements to choose from. The orthogonality across M_{t} transmit channels can theoretically be guaranteed by any set of M_{t} Doppler shifts. What is more, any set of consecutive M_{t} Doppler shifts results in the same beamformed mainlobe directions except for a different extra phase, thus making no difference to the transmit beampattern. As an example for discussion, the first M_{t} Doppler shifts are chosen for phase modulation by default in this paper. In this case, phase modulation vector for a transmitter of M_{t} elements can be expressed as the following $M_{\mathrm{t}}\times 1$ vector

$$\mathbf{w}_{\mathrm{TB},q}=\left[1,e^{-j2\pi\frac{q-1}{M_{\mathrm{v}}}},\ldots,e^{-j2\pi\frac{(M_{\mathrm{t}}-1)(q-1)}{M_{\mathrm{v}}}}\right]^{T}. \tag{19}$$

Equations (16) and (19) make it clear that a larger M_{v} leads to smaller mainlobe distances between adjacent pulse beams. As a result, more pulse beams are directed toward a fixed spatial sector. Assuming that $\mathbf{\Theta}$ is known *a priori*, there are $M<M_{\mathrm{v}}$ pulses whose beam mainlobes are directed toward $\mathbf{\Theta}$ in every M_{v} pulses, and the index vector of these M pulses from the first pulse period is denoted as $\mathbf{q}_{\mathrm{v}}=[q_1,q_2,\ldots,q_M]$. To focus the transmit energy within $\mathbf{\Theta}$, only the modulation vectors of these M pulses are selected to constitute a new phase modulation matrix $\mathbf{W}_{\mathrm{TB}}\in\mathbb{C}^{M_{\mathrm{t}}\times Q}$ for slow-time TB MIMO radar, which is given by

$$\begin{aligned} &\mathbf{W}_{\mathrm{TB},0}\triangleq\left[\mathbf{w}_{\mathrm{TB},q_1},\mathbf{w}_{\mathrm{TB},q_2},\ldots,\mathbf{w}_{\mathrm{TB},q_M}\right]\in\mathbb{C}^{M_{\mathrm{t}}\times M} \\ &\mathbf{W}_{\mathrm{TB}}\triangleq\left[\underbrace{\mathbf{W}_{\mathrm{TB},0},\mathbf{W}_{\mathrm{TB},0},\ldots,\mathbf{W}_{\mathrm{TB},0}}_{Q/M}\right] \end{aligned} \tag{20}$$

where Q/M is assumed to be an integer, and the qth column vector of $\mathbf{W}_{\mathrm{TB}}$ is used for the qth pulse. Building a new phase modulation matrix that only includes modulation vectors whose mainlobes are directed toward the desired region allows to focus

the transmit energy within $\boldsymbol{\Theta}$, resulting in energy distribution optimization.

As it is stated in Section II-B, after the separation of subarray signals, signals from different subarrays can be treated as independent signals, and azimuth and elevation can be estimated separately. Therefore, based on the spatial region of interest, slow-time phase modulation matrices $\mathbf{W}_{\mathrm{x,TB}}$ for x-subarray and $\mathbf{W}_{\mathrm{z,TB}}$ for z-subarray can be designed independently for beamspace optimization.

B. Doppler Spectrum for Slow-Time Transmit Beamspace MIMO Radar

DDMA technique takes advantage of the divisibility between different channel signals in the Doppler domain to achieve waveform diversity. With a DDMA phase modulation matrix, each transmit channel is modulated with a distinct shift in the Doppler domain. To be more specific, after DDMA modulation, the signal energy of each channel for a target is focused on a single peak and at a different location from the other channels in the Doppler domain, which is the basis for channel separation. However, this condition does not hold for the case of slow-time TB technique.

Observing (3) and (20), we can see that the mth transmit channel in a CPI of Q pulses is modulated with Q elements in the mth row of a modulation matrix. Denote the mth row of DDMA modulation matrix $\mathbf{W}$ as

$$\mathbf{v}_m = \left[1, e^{-j2\pi\frac{(m-1)\mathrm{PRF}}{M_{\mathrm{v}}}T_{\mathrm{r}}}, \ldots, e^{-j2\pi\frac{(m-1)\mathrm{PRF}}{M_{\mathrm{v}}}(Q-1)T_{\mathrm{r}}}\right], \tag{21}$$

and the mth row of the proposed slow-time TB matrix $\mathbf{W}_{\mathrm{TB}}$ as

$$\mathbf{v}_{\mathrm{TB},m} \triangleq \left[\underbrace{\mathbf{v}_0, \mathbf{v}_0, \ldots, \mathbf{v}_0}_{Q/M}\right] \in \mathbb{C}^{1\times Q}. \tag{22}$$

Here

$$\begin{aligned}\mathbf{v}_0 &= e^{-j2\pi\frac{(m-1)\mathrm{PRF}}{M_{\mathrm{v}}}T_{\mathrm{r}}[q_1-1, q_2-1, \ldots, q_M-1]} \\ &= e^{-j2\pi\frac{(m-1)\mathrm{PRF}}{M_{\mathrm{v}}}T_{\mathrm{r}}(\mathbf{q}_{\mathrm{v}}-\mathbf{1})} \in \mathbb{C}^{1\times M}\end{aligned} \tag{23}$$

where $\mathbf{1}$ is an all-ones vector of the same size as $\mathbf{q}_{\mathrm{v}}$. According to (21), DDMA technique works by multiplying each transmit channel signal with a distinct complex sinusoid [44] in slow time domain (across pulses), whose frequency is $f_{\mathrm{v},m} = (m-1)\mathrm{PRF}/M_{\mathrm{v}}, m = 1, 2, \ldots, M_{\mathrm{t}}$, and its sampling rate is $1/T_{\mathrm{r}} = \mathrm{PRF}$. A signal, multiplication (element-wise product) by a complex sinusoid of frequency $f_{\mathrm{v},m}$ is equivalent to shifting it in the Doppler domain by $f_{\mathrm{v},m}$. As a result of such a shift, if the original signal energy focuses on a single peak, the modulated signal will also spread on only one peak, and its location depends on the amount of Doppler shift. Therefore, M_{t} transmit channel signals for the same target will be distributed on M_{t} separate peaks when using DDMA technique.

In contrast, for every period of M_{v} pulse vectors, the slow-time TB technique described in (22) and (23) only uses those M DDMA modulation pulse vectors whose beam mainlobes are directed toward the desired spatial region, discarding the remaining pulse vectors. As a result, the signal composed of Q sample points used for slow-time TB modulation is no longer a complex sinusoid, albeit remaining periodical with a period of M pulses.

According to the Fourier analysis of a periodical signal $\mathrm{f}(t)$, with the Fourier decomposition

$$\mathrm{f}(t) = \sum_{n=-\infty}^{\infty} a_n e^{j2\pi n f_0 t} \tag{24}$$

where t denotes the time index, a_n is the Fourier coefficient, n is an integer, and $1/f_0$ is the period of signal $\mathrm{f}(t)$, the slow-time TB modulation signal can be viewed as a superstition of multiple complex sinusoids with different frequencies. Therefore, using slow-time TB technique, a transmit channel can be considered to be modulated with multiple different Doppler shifts simultaneously, and these Doppler shift values are $\{n/(MT_{\mathrm{r}})\}_{n=-\infty}^{\infty}$. As a result of slow-time TB modulation, the signal energy of one transmit channel for a target is scattered on more than one Doppler peak, and its peak positions coincide with those of other channels. Signals from distinct transmit channels are mixed up and overlap with each other in the Doppler domain, making it impossible to separate transmit channels using Doppler spectrum division.

Nearly all DOA estimation algorithms, including MUSIC, ESPRIT, and conventional CPD methods [38], are based on the assumption that M_{t} separated transmit channel signals can be obtained by signal processing procedures before DOA estimation, such as Doppler spectrum division for DDMA. As previously concluded, transmit signals employing slow-time TB technique are no longer separable in the Doppler domain, rendering the algorithms mentioned above invalid. To handle this issue and take advantage of the tensor-based model as well, a method using CPD without Doppler spectrum division is proposed for slow-time TB MIMO radar to achieve parameter estimation, which is described in detail in the next section.

IV. Parameter Estimation Using CPD for L-Shaped Array

In this section, we present a new tensor-based signal model and a new parameter estimation method using this model for the proposed slow-time TB L-shaped MIMO radar. This method avoids transmit channel separation. Moreover, it fully leverages the multi-linear structure inherent in the signal to improve estimation performance and resolve velocity ambiguity issue. Section IV-A explains the CPD algorithm for the traditional DDMA modulation technique as a basis for comparison, while Section IV-B presents the proposed tensor-based signal model and parameter estimation algorithm.

A. CPD for DDMA L-Shaped Array

To achieve the objective of separating the DDMA signal from each transmit channel within a subarray, phase demodulation is implemented by first shifting the received signal from M_{L}

transmit elements back to the baseband in the Doppler domain, which is done with Doppler shifts $-(m-1)\mathrm{PRF}/M_{\mathrm{L}}, m=1,2,\ldots,M_{\mathrm{L}}$, respectively, where $M_{\mathrm{x}}=M_{\mathrm{z}}=M_{\mathrm{L}}$ is assumed for simplicity in this section. After lowpass filtering with cutoff frequency $\mathrm{PRF}/M_{\mathrm{L}}/2$, signals of $M_{\mathrm{L}}M_{\mathrm{r}}$ virtual transmit-receive channels for each ULA subarray are obtained. After separation, the signals from the (m,n)-th transmit-receive channels of x-axis and z-axis subarrays for the $\overline{q}$th pulse can be written as, respectively,

$$\begin{aligned} y_{\mathrm{x},mn\overline{q}} &= \sum_{k=1}^{K}\sigma_k e^{j2\pi f_k(\overline{q}-1)T_{\mathrm{r}}}a_{\mathrm{x},m}\left(\varphi_k\right)b_n\left(\varphi_k,\phi_k\right)+z_{\mathrm{x},mn\overline{q}} \\ y_{\mathrm{z},mn\overline{q}} &= \sum_{k=1}^{K}\sigma_k e^{j2\pi f_k(\overline{q}-1)T_{\mathrm{r}}}a_{\mathrm{z},m}\left(\phi_k\right)b_n\left(\varphi_k,\phi_k\right)+z_{\mathrm{z},,mn\overline{q}} \end{aligned} \tag{25}$$

where $a_{\mathrm{x},m}\left(\varphi_k\right)$ and $a_{\mathrm{z},m}\left(\phi_k\right)$ are the mth elements of $\mathbf{a}_{\mathrm{x}}\left(\varphi_k\right)$ and $\mathbf{a}_{\mathrm{z}}\left(\phi_k\right)$, respectively, and $z_{\mathrm{x},,mn\overline{q}}$ and $z_{\mathrm{z},,mn\overline{q}}$ are the noise components of two subarray channels. Considering that the number of pulse samples is decreased by M_{L} times after Doppler spectrum division, $\overline{q}$ instead of q is used in (25), and $\overline{q}=1,1+M_{\mathrm{L}},\ldots,1+M_{\mathrm{L}}(P-1)$, where $P=Q/M_{\mathrm{L}}$ is assumed to be an integer.

Storing the separated signals in (25) in 3-dimensional (3-D) tensors, we have

$$\begin{aligned} \mathcal{Y}_{\mathrm{x}} &= \sum_{k=1}^{K}\sigma_k\mathbf{a}_{\mathrm{x}}\left(\varphi_k\right)\circ\mathbf{b}\left(\varphi_k,\phi_k\right)\circ\overline{\mathbf{d}}\left(f_k\right)+\mathcal{Z}_{\mathrm{x}} \\ \mathcal{Y}_{\mathrm{z}} &= \sum_{k=1}^{K}\sigma_k\mathbf{a}_{\mathrm{z}}\left(\phi_k\right)\circ\mathbf{b}\left(\varphi_k,\phi_k\right)\circ\overline{\mathbf{d}}\left(f_k\right)+\mathcal{Z}_{\mathrm{z}} \end{aligned} \tag{26}$$

where $\circ$ denotes the outer product of matrices, $\mathcal{Z}_{\mathrm{x}}$ and $\mathcal{Z}_{\mathrm{z}}$ are the noise tensors, and $\overline{\mathbf{d}}\left(f_k\right)$ is given by

$$\overline{\mathbf{d}}\left(f_k\right)\triangleq\left[d_1\left(f_k\right),d_{1+M_{\mathrm{L}}}\left(f_k\right),\ldots,d_{1+M_{\mathrm{L}}(P-1)}\left(f_k\right)\right]^T \tag{27}$$

where

$$d_q\left(f_k\right)=e^{j2\pi f_k(q-1)T_{\mathrm{r}}},q=1,2,\ldots,Q. \tag{28}$$

Factor matrices $\mathbf{A}_{\mathrm{x}}$, $\mathbf{A}_{\mathrm{z}}$, $\mathbf{B}$, and $\overline{\mathbf{D}}$ of the constructed tensors can be defined as

$$\begin{aligned} \mathbf{A}_{\mathrm{x}} &\triangleq \left[\mathbf{a}_{\mathrm{x}}\left(\varphi_1\right),\mathbf{a}_{\mathrm{x}}\left(\varphi_2\right),\ldots,\mathbf{a}_{\mathrm{x}}\left(\varphi_K\right)\right] \\ \mathbf{A}_{\mathrm{z}} &\triangleq \left[\mathbf{a}_{\mathrm{z}}\left(\phi_1\right),\mathbf{a}_{\mathrm{z}}\left(\phi_2\right),\ldots,\mathbf{a}_{\mathrm{z}}\left(\phi_K\right)\right] \\ \mathbf{B} &\triangleq \left[\mathbf{b}\left(\varphi_1,\phi_1\right),\mathbf{b}\left(\varphi_2,\phi_2\right),\ldots,\mathbf{b}\left(\varphi_K,\phi_K\right)\right] \\ \overline{\mathbf{D}} &\triangleq \left[\overline{\mathbf{d}}\left(f_1\right),\overline{\mathbf{d}}\left(f_2\right),\ldots,\overline{\mathbf{d}}\left(f_K\right)\right]. \end{aligned} \tag{29}$$

To obtain the factor matrices in (29), the CPD approach via ALS is employed. Taking the factor matrix $\mathbf{A}_{\mathrm{x}}$ as an example, the problem of estimating $\mathbf{A}_{\mathrm{x}}$ boils down to solving the following optimization (data fitting) problem

$$\hat{\mathbf{A}}_{\mathrm{x}}\leftarrow\arg\min_{\mathbf{A}_{\mathrm{x}}}\left\|\left[\mathcal{Y}_{\mathrm{x}}\right]_{(1)}-\left[(\mathbf{B}\odot\overline{\mathbf{D}})\mathbf{A}_{\mathrm{x}}^T\right]\right\|_F^2 \tag{30}$$

where $[\cdot]_{(1)}$ is the mode-1 unfolding of a tensor, $\odot$ stands for the Khatri-Rao product (or column-wise Kronecker product) of matrices, and $||\cdot||_F$ denotes the Frobenius norm of a matrix. As a result, 2-D DOAs can be estimated using traditional ULA DOA estimation methods, such as ESPRIT, with the obtained $\hat{\mathbf{A}}_{\mathrm{x}}$ and $\hat{\mathbf{A}}_{\mathrm{z}}$.

B. CPD for Slow-Time Transmit Beamspace L-Shaped Array

As shown in Section IV-A, the CPD method can give DOA estimates for DDMA L-shaped array radar. However, Doppler spectrum division operation, which is required prior to CPD operation, results in pulse signal downsampling. As a result, the useful velocity information contained in the pulse signal measurements is lost partly, and velocity ambiguity arises when the factor matrix $\overline{\mathbf{D}}$ in (29) is used to estimate target velocity. On the other hand, DDMA phase modulation matrix $\mathbf{W}$, whose column vectors function as beamformers, distributes the transmit energy over the whole spatial region and does not allow for energy focusing. Considering the above issues, a new method called slow-time TB L-shaped array based on CPD is proposed, which enables velocity disambiguation and performance improvement of parameter estimation.

To focus transmit energy within the region of interest $\mathbf{\Theta}$, slow-time phase modulation matrices $\mathbf{W}_{\mathrm{x,TB}}$ and $\mathbf{W}_{\mathrm{z,TB}}$ are designed first. Storing the received signals of subarrays in matrices $\mathbf{Y}_{\mathrm{x}}$ and $\mathbf{Y}_{\mathrm{z}}$ both of size $M_{\mathrm{r}}\times Q$, we have

$$\begin{aligned} \mathbf{Y}_{\mathrm{x}} &= (\mathbf{p}\odot\mathbf{B})\left[\left(\mathbf{W}_{\mathrm{x,TB}}^T\mathbf{A}_{\mathrm{x}}\right)*\mathbf{D}\right]^T+\mathbf{Z}_{\mathrm{x}} \\ \mathbf{Y}_{\mathrm{z}} &= (\mathbf{p}\odot\mathbf{B})\left[\left(\mathbf{W}_{\mathrm{z,TB}}^T\mathbf{A}_{\mathrm{z}}\right)*\mathbf{D}\right]^T+\mathbf{Z}_{\mathrm{z}} \end{aligned} \tag{31}$$

where $\mathbf{p}=[\sigma_1,\sigma_2,\ldots,\sigma_K]$, $*$ denotes the Hadamard product of matrices, and

$$\begin{aligned} \mathbf{D} &\triangleq \left[\mathbf{d}\left(f_1\right),\mathbf{d}\left(f_2\right),\ldots,\mathbf{d}\left(f_K\right)\right] \\ \mathbf{d}\left(f_k\right) &\triangleq \left[d_1\left(f_k\right),d_2\left(f_k\right),\ldots,d_Q\left(f_k\right)\right]^T. \end{aligned} \tag{32}$$

The (n,q)-th elements of matrices $\mathbf{Z}_{\mathrm{x}}$ and $\mathbf{Z}_{\mathrm{z}}$ are $z_{\mathrm{x},nq}$ and $z_{\mathrm{z},nq}$ in (13), respectively. Taking advantage of the periodicity of the phase modulation matrices $\mathbf{W}_{\mathrm{x,TB}}$ and $\mathbf{W}_{\mathrm{z,TB}}$, (31) can be re-expressed as

$$\begin{aligned} \mathbf{Y}_{\mathrm{x}} &= (\mathbf{p}\odot\mathbf{B})\left[\overline{\mathbf{H}}\odot\mathbf{A}_{\mathrm{x,TB}}\right]^T+\mathbf{Z}_{\mathrm{x}} \\ \mathbf{Y}_{\mathrm{z}} &= (\mathbf{p}\odot\mathbf{B})\left[\overline{\mathbf{H}}\odot\mathbf{A}_{\mathrm{z,TB}}\right]^T+\mathbf{Z}_{\mathrm{z}} \end{aligned} \tag{33}$$

where $\overline{\mathbf{H}}\triangleq\left[\overline{\mathbf{h}}\left(f_1\right),\overline{\mathbf{h}}\left(f_2\right),\ldots,\overline{\mathbf{h}}\left(f_K\right)\right]$, and $\overline{\mathbf{h}}\left(f_k\right)$ is given by

$$\overline{\mathbf{h}}\left(f_k\right)\triangleq\left[d_1\left(f_k\right),d_{1+M}\left(f_k\right),\ldots,d_{1+M(P_{\mathrm{v}}-1)}\left(f_k\right)\right]^T \tag{34}$$

where $P_{\mathrm{v}}=Q/M$ is an integer. Matrices $\mathbf{A}_{\mathrm{x,TB}}$ and $\mathbf{A}_{\mathrm{z,TB}}$ can be further expressed as

$$\begin{aligned} \mathbf{A}_{\mathrm{x,TB}} &= \left(\mathbf{W}_{\mathrm{x,TB},0}^T\mathbf{A}_{\mathrm{x}}\right)*\mathbf{D}_0 \\ \mathbf{A}_{\mathrm{z,TB}} &= \left(\mathbf{W}_{\mathrm{z,TB},0}^T\mathbf{A}_{\mathrm{z}}\right)*\mathbf{D}_0 \end{aligned} \tag{35}$$

where $\mathbf{W}_{\mathrm{x,TB},0}$ and $\mathbf{W}_{\mathrm{z,TB},0}$ are defined in the same way as $\mathbf{W}_{\mathrm{TB},0}$ in (20), and $\mathbf{D}_0$ consists of the first M rows of $\mathbf{D}$.

Taking the signal $\mathbf{Y}_{\mathrm{x}}$ in (33) as an example, the signal transformation from a matrix into a 3-D tensor of size $M\times M_{\mathrm{r}}\times P_{\mathrm{v}}$ is illustrated in Fig. 2. Then we have

$$\mathcal{Y}_{\mathrm{x,D}}=\sum_{k=1}^{K}\sigma_k\mathbf{a}_{\mathrm{x,TB}}\left(\varphi_k\right)\circ\mathbf{b}\left(\varphi_k,\phi_k\right)\circ\overline{\mathbf{h}}\left(f_k\right)+\mathcal{Z}_{\mathrm{x,D}}$$

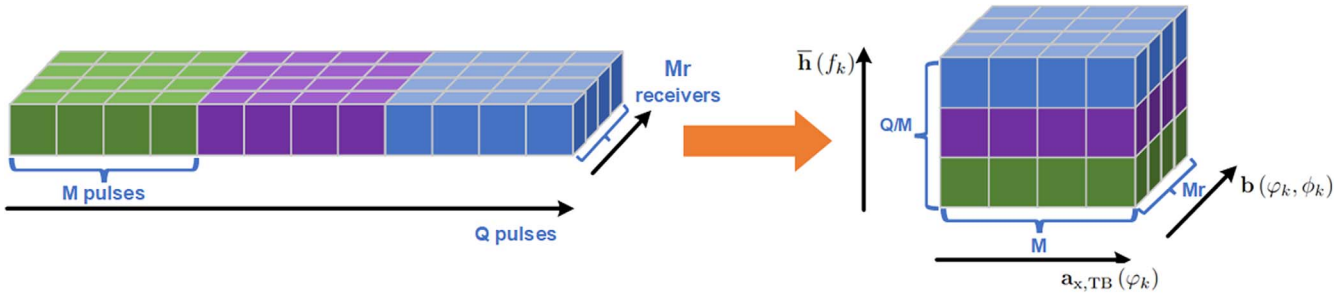

Fig. 2. Illustration of transforming a matrix signal into a 3-D tensor.

$$\mathcal{Y}_{\mathrm{z,D}} = \sum_{k=1}^{K} \sigma_k \mathbf{a}_{\mathrm{z,TB}}(\phi_k) \circ \mathbf{b}(\varphi_k, \phi_k) \circ \overline{\mathbf{h}}(f_k) + \mathcal{Z}_{\mathrm{z,D}} \quad (36)$$

where $\mathcal{Z}_{\mathrm{x,D}}$ and $\mathcal{Z}_{\mathrm{z,D}}$ are noise tensors.

Comparing (26) with (36), the part of velocity information that is lost in (26) is preserved in (36), that is,

$$\begin{aligned}\mathbf{A}_{\mathrm{x,TB}} &\triangleq [\mathbf{a}_{\mathrm{x,TB}}(\varphi_1), \mathbf{a}_{\mathrm{x,TB}}(\varphi_2), \ldots, \mathbf{a}_{\mathrm{x,TB}}(\varphi_K)] \\ \mathbf{A}_{\mathrm{z,TB}} &\triangleq [\mathbf{a}_{\mathrm{z,TB}}(\phi_1), \mathbf{a}_{\mathrm{z,TB}}(\phi_2), \ldots, \mathbf{a}_{\mathrm{z,TB}}(\phi_K)]. \end{aligned} \quad (37)$$

Thus, the unambiguous velocity can be restored by combining $\overline{\mathbf{H}}$ with $\mathbf{D}_0$ contained in $\mathbf{A}_{\mathrm{x,TB}}$ or $\mathbf{A}_{\mathrm{z,TB}}$.

With factor matrices $\mathbf{A}_{\mathrm{x,TB}}$, $\mathbf{A}_{\mathrm{z,TB}}$ and $\overline{\mathbf{H}}$ obtained by CPD, the minimum mean square error (MMSE) estimation algorithm can be employed to estimate DOA pairs $\{\varphi_k, \phi_k\}_{k=1}^K$. Looking into (35), we can find that $\mathbf{A}_{\mathrm{x,TB}}$ is the Hadamard product of $\mathbf{D}_0$ and $\mathbf{E}_{\mathrm{x}} = \mathbf{W}_{\mathrm{x,TB},0}^T \mathbf{A}_{\mathrm{x}}$. For the kth column of $\mathbf{E}_{\mathrm{x}}$, we can write

$$\begin{aligned}\mathbf{e}_{\mathrm{x},k} &= \mathbf{W}_{\mathrm{x,TB},0}^T \mathbf{a}_{\mathrm{x}}(\varphi_k) \\ &= \left[\mathbf{w}_{\mathrm{x,TB},q_1}^T \mathbf{a}_{\mathrm{x}}(\varphi_k), \mathbf{w}_{\mathrm{x,TB},q_2}^T \mathbf{a}_{\mathrm{x}}(\varphi_k), \ldots, \mathbf{w}_{\mathrm{x,TB},q_M}^T \mathbf{a}_{\mathrm{x}}(\varphi_k)\right]^T \end{aligned} \quad (38)$$

where $\mathbf{w}_{\mathrm{x,TB},q_m}$ is the mth column of $\mathbf{W}_{\mathrm{x,TB},0}$. Considering that each TB phase modulation vector $\mathbf{w}_{\mathrm{x,TB},q_m}$ obeys the discrete Fourier transform (DFT) structure for different frequencies $f_{q_m} = (q_m - 1)/M_{\mathrm{v}}, q_m = q_1, q_2, \ldots, q_M$, $\mathbf{e}_{\mathrm{x},k}$ can be regarded as DFT operations at M different frequency points. Meanwhile, every element of $\mathbf{D}_0$ is an exponential value with unit amplitude, having no effect on the element amplitudes of $\mathbf{A}_{\mathrm{x,TB}}$. Therefore, $\{\varphi_k\}_{k=1}^K$ can be estimated by solving the following MMSE problem

$$\hat{\varphi}_k = \arg\min_{\varphi} \| |\mathbf{e}_{\mathrm{x},k}| - |\mathbf{e}(\varphi)| \|_F^2 \quad (39)$$

where $\mathbf{e}(\varphi) = \mathbf{W}_{\mathrm{x,TB},0}^T \mathbf{a}_{\mathrm{x}}(\varphi)$. In a similar way, $\{\phi_k\}_{k=1}^K$ can be estimated as well.

To obtain unambiguous velocity, the estimated factor $\hat{\overline{\mathbf{H}}}$ is combined with $\mathbf{D}_0$, and $\mathbf{D}_0$ is estimated by

$$\hat{\mathbf{D}}_0 = \mathbf{A}_{\mathrm{x,TB}} \oslash \hat{\mathbf{E}}_{\mathrm{x}} \quad (40)$$

where $\oslash$ denotes the element-wise division of two matrices. $\hat{\mathbf{E}}_{\mathrm{x}}$ is the estimate of $\mathbf{E}_{\mathrm{x}}$ by substituting $\{\hat{\varphi}_k\}_{k=1}^K$ in (38). With $\hat{\overline{\mathbf{H}}}$ and $\hat{\mathbf{D}}_0$, we can find

$$\hat{\overline{\mathbf{H}}} \odot \hat{\mathbf{D}}_0 \triangleq [\mathbf{d}(f_1), \mathbf{d}(f_2), \ldots, \mathbf{d}(f_K)]. \quad (41)$$

From (41), target velocities $\{v_k\}_{k=1}^K$ can then be easily obtained.

As discussed above, 2-D DOA estimation for the proposed L-shaped array slow-time MIMO TB radar is achieved by estimating azimuth and elevation separately. Consequently, 2-D DOA pair-matching is required in the presence of more than one target. Recalling (36), factor matrices $\mathbf{A}_{\mathrm{x,TB}}$, $\mathbf{A}_{\mathrm{z,TB}}$, and $\mathbf{B}$ are obtained after tensor decomposition via ALS. However, only the matrices associated with transmit arrays, i.e., $\mathbf{A}_{\mathrm{x,TB}}$ and $\mathbf{A}_{\mathrm{z,TB}}$, are utilized for DOA estimation, while factor matrix $\mathbf{B}$ associated with the receive array is not utilized.[4] According to the PARAFAC uniqueness conditions given in terms of Kruskal rank [45], these factor matrices are unique up to permutation and scaling of columns if the following inequalities are satisfied

$$\begin{aligned} r_{\mathbf{A}_{\mathrm{x,TB}}} + r_{\overline{\mathbf{H}}} + r_{\mathbf{B}} &\geq 2K + 2 \\ r_{\mathbf{A}_{\mathrm{z,TB}}} + r_{\overline{\mathbf{H}}} + r_{\mathbf{B}} &\geq 2K + 2 \end{aligned} \quad (42)$$

where $r_{\{\cdot\}}$ denotes the Kruskal rank of a matrix. Therefore, the parameters estimated based on these factor matrices are automatically paired column-by-column if (42) holds. Thanks to this property, factor matrix $\mathbf{B}$ can be utilized for pair-matching. Given that two transmit subarrays in the proposed L-shaped array arrangement can already give 2-D DOA estimation except for pair-matching, the receive array's shape has no effect on pair-matching capability. A concrete example is given and discussed in Section V.

Finally, the DOA pairs $\{\varphi_k, \phi_k\}_{k=1}^K$ can be found with performance improvement as will be validated in the next section, and velocity ambiguity can be resolved at the same time.

V. Simulation Results

In this section, simulation experiments are conducted to demonstrate the effectiveness of the proposed slow-time TB method for pulsed L-shaped array MIMO radar with frequency-modulated continuous waves in the scenario of automotive radar applications. Throughout all the simulations, we assume an L-shaped transmit array where two ULA subarrays are positioned along the x-axis and z-axis, and each subarray is made up of $M_{\mathrm{L}} = M_{\mathrm{x}} = M_{\mathrm{z}} = 8$ antenna elements spaced half a wavelength apart from each other. The receiver, which is collocated with the transmitter, is set as a ULA along the x-axis with

[4] It is because the estimate based on the factor matrices $\mathbf{A}_{\mathrm{x,TB}}$ consistently outperforms the estimate based on $\mathbf{B}$ in all our simulations.

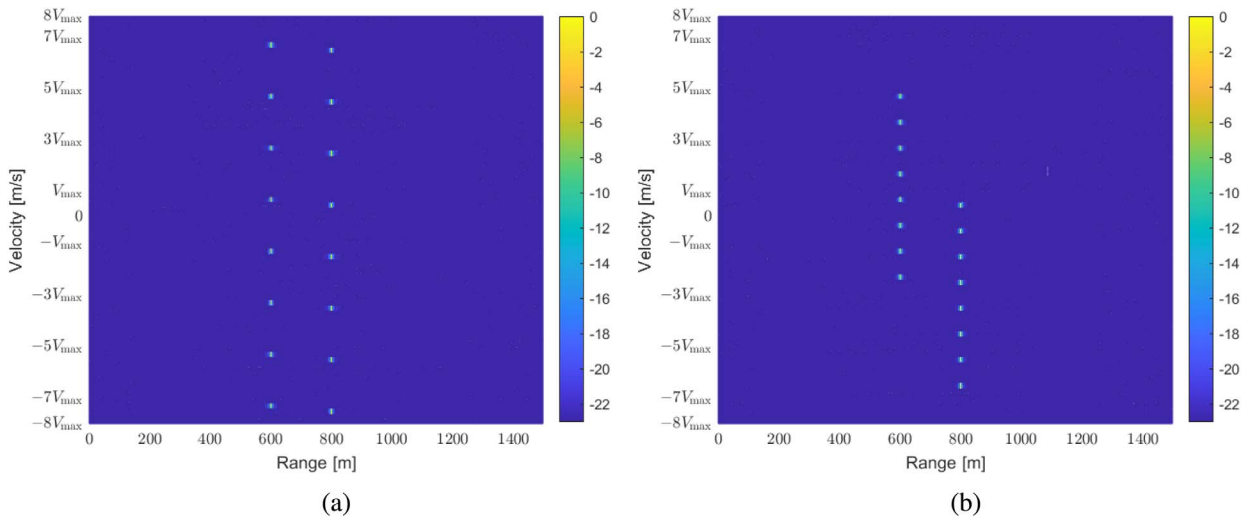

Fig. 3. Range-Doppler map of DDMA approach with (a) $M_{\rm v} = M_{\rm L}$ and (b) $M_{\rm v} > M_{\rm L}$.

$M_{\rm r} = 8$ elements and the spacing between adjacent elements $d_{\rm r} = \lambda/2$ in simulations for demonstration.[5] The frequency of carrier waveform is $f_{\rm c} = 79$ GHz, and the transmit signal is sampled with sampling frequency $f_{\rm s} = 70$ MHz. We also set $Q = 80$ pulses with $T_{\rm r} = 10$ us in a single CPI, and each pulse duration is $T_{\rm p} = 3$ us. It is assumed that source targets follow the Swerling I model, and the additive noise is Gaussian zero-mean unit-variance spatially and temporally white.

A. Example 1: Comparison Between DDMA and Slow-Time Transmit Beamspace Approaches

In this example, there are 2 moving targets with ranges $\mathbf{R} = \{800\ {\rm m}, 600\ {\rm m}\}$ and velocities $\mathbf{v} = \{0.4v_{\max}, 4.6v_{\max}\}$, where $v_{\max} = \lambda {\rm PRF}/4/{\rm M_L} = 11.87\ {\rm m/s}$ is the maximum unambiguous velocity for DDMA. The value of $v_{\max}$ remains constant throughout this section without any special remarks. To demonstrate the range-Doppler map of the received signal, down & up chirp signals (see (43)) are used for two subarrays as baseband transmit waveforms

$$\mathrm{u}_i(t) = \mathrm{rect}\left(\frac{t - T_{\rm p}/2}{T_{\rm p}}\right) e^{j\pi K_i t^2}, \quad i = 1, 2 \tag{43}$$

where $K_1 = -B/T_{\rm p}$ and $K_2 = B/T_{\rm p}$ are the chirp rates for down-chirp and up-chirp signals, respectively, and the transmit signal bandwidth is $B = 60$ MHz throughout this section.

The phase modulation matrix for DDMA approach is described in (3) with $M_{\rm t} = M_{\rm L} = 8$. After 2-D DFT, the range-Doppler map of the received signal is depicted in Fig. 3(a). With DDMA phase modulation, the signal from each transmit element is modulated with a distinct Doppler shift. Therefore, as it can be seen in Fig. 3(a), 8 separate peaks are uniformly distributed over the entire Doppler spectrum along an identical range cell for each target. Each peak can be regarded as attributed to the signal from only one transmit element, which ensures that waveform diversity can be achieved by Doppler spectrum division.

To enhance the performance of MIMO radar further, as discussed in Section III, a new phase modulation matrix is proposed that optimizes the transmit energy distribution. The region of interest is set as $\mathbf{\Theta} = [60^\circ, 120^\circ]$ throughout this section. First, the entire spectrum is divided into $M_{\rm v} = 16$ subbands in this example, which narrows down the mainlobe distance of adjacent beams formed by phase modulation vectors compared to conventional DDMA with $M_{\rm v} = 8$, and its range-Doppler map is given in Fig. 3(b). Observing two figures in Fig. 3, we can see that peaks are distributed uniformly for both of them, while the distance of adjacent peaks gets smaller, and there exists an extra Doppler spectrum band for the DDMA with $M_{\rm v} = 16$ in Fig. 3(b) due to the fact that $M_{\rm v} > M_{\rm t}$. Next, those modulation vectors of pulses $\{1, 2, 3, 4, 13, 14, 15, 16\}$ in every period of 16 pulses are selected to construct a new phase modulation for transmit energy optimization. The transmit energy distribution of conventional DDMA and the proposed approach are demonstrated in Fig. 4. Compared to DDMA approach in Fig. 4(a), adjacent beams of the proposed approach in Fig. 4(b) get closer to each other, resulting in more beams directing toward $\mathbf{\Theta}$. By selecting those pulse vectors whose beamforming mainlobes direct toward $\mathbf{\Theta}$, the overall transmit energy of the proposed approach in a pulse period is no longer spread across the whole spatial region as it is in the conventional DDMA technique, and instead the proposed method achieves transmit energy optimization: its transmit energy accumulates within $\mathbf{\Theta}$.

Different from DDMA technique, as it is discussed in Section III-B, the separation of transmit channels for the proposed slow-time TB technique cannot be achieved by Doppler spectrum division because the energy of a single transmit channel for each target can be distributed over multiple peaks in the Doppler domain rather than one single cluster of range-Doppler bins and mixed up with those peaks of other channels. Fig. 5(a) depicts the received signal with the proposed TB modulation matrix $\mathbf{W}_{\rm TB}$ in the Doppler domain. Compared to DDMA in Fig. 3(a),

[5]The receiver does not have to be an ULA with $\lambda/2$ spacing.

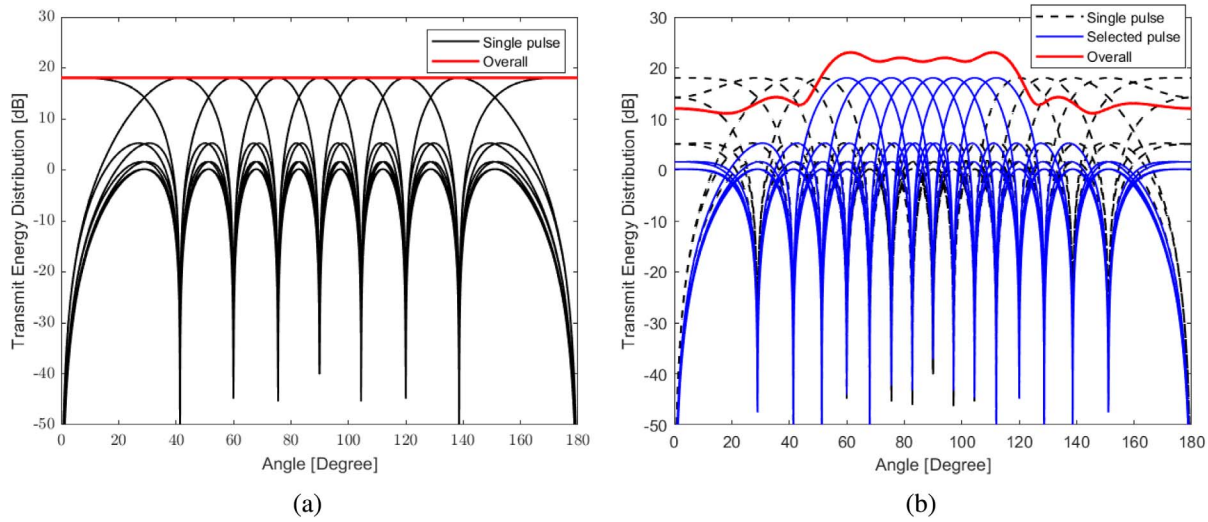

Fig. 4. Transmit energy beampatterns of (a) DDMA and (b) the proposed approach.

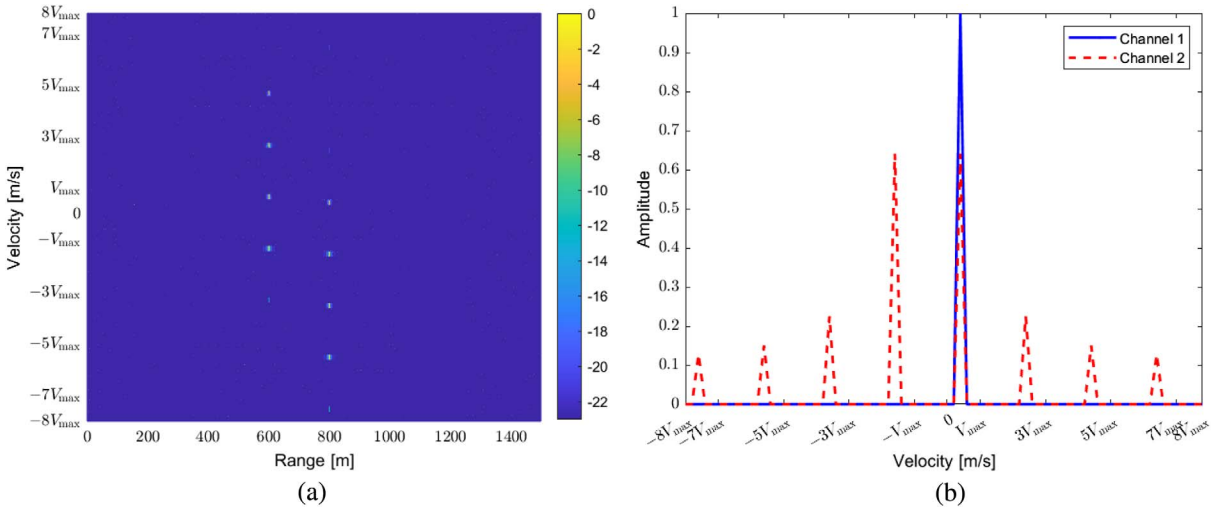

Fig. 5. (a) Range-Doppler map of the proposed approach and (b) Doppler spectrums of two transmit channels.

there are the same number of peaks as DDMA for a target in the Doppler domain, but amplitudes of these peaks differ a lot from each other. Taking the first and second transmit channels of the first target as an example, their Doppler spectrums are shown in Fig. 5(b). For the first transmit channel, its energy only accumulates over one peak due to zero Doppler shift, and the energy dispersed over other regions is so low as to be ignored. In contrast, the signal of the second channel is spread over 8 peaks with uniform distances but different amplitudes, which verifies the analysis in Section III-B. As a consequence, waveform diversity cannot be achieved by Doppler spectrum division. Therefore, conventional parameter estimation algorithms including MUSIC, ESPRIT, and CPD in [38] no longer work. To obtain both transmit energy distribution optimization and parameter estimation, a new parameter estimation method based on CPD is proposed, and its performance is evaluated in Section V-C.

B. Example 2: Discussion on M_{v}

A larger M_{v} narrows down the mainlobe interval between adjacent beams, which consequently directs more beams within the region of interest $\boldsymbol{\Theta}$. With a predetermined $\boldsymbol{\Theta}$, any $M_{\mathrm{v}} > M_{\mathrm{t}}$ can achieve transmit energy focusing by proper pulse selection, and different M_{v} leads to a different transmit energy beampattern. To evaluate the performance of transmit energy distribution optimization, here we define the average energy per pulse coming from within $\boldsymbol{\Theta}$ as the transmit beamspace energy P, which can be expressed as

$$P = \frac{1}{M} \sum_{q \in \mathcal{I}} \int_{\boldsymbol{\Theta}} \left| \mathbf{a}^T(\theta) \mathbf{w}_q \right|^2 d\theta \tag{44}$$

where M is the number of selected pulses of each period for slow-time TB MIMO radar, and $\mathcal{I}$ is the index set of the selected pulses.

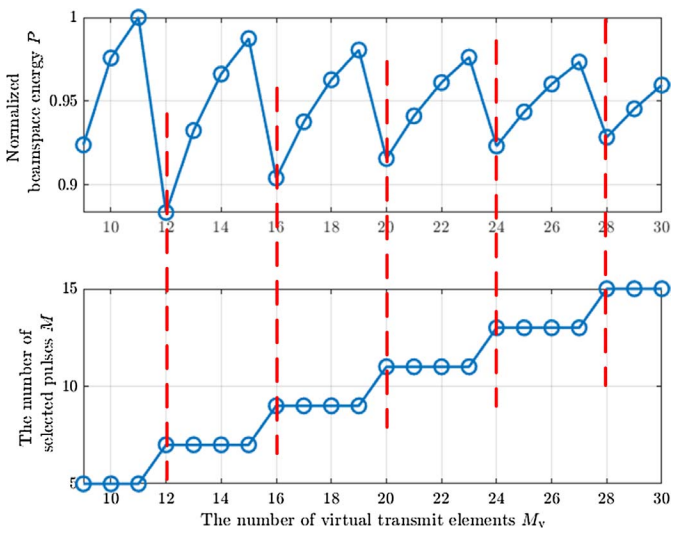

Fig. 6. Beamspace energy P and the number of selected pulses M within each pulse period versus M_{v}.

To illustrate the different beamspace beampatterns for different M_{v}, consider the following example. If the mainlobe direction formed by a pulse vector satisfies $\theta_{\mathrm{b},q} \in \mathbf{\Theta}$, its phase modulation vector is selected to construct a new phase modulation matrix for slow-time TB MIMO radar. Taking $M_{\mathrm{v}} = 16$ as an example, 9 modulation pulse vectors within a period of 16 pulses are selected, and their pulse index set is $\mathcal{I} = \{1, 2, 3, 4, 5, 13, 14, 15, 16\}$, and the corresponding mainlobe directions $\{\cos\theta_{\mathrm{b},q}\}_{q\in\mathcal{I}}$, defined in (16) with $M_{\mathrm{t}} = 16$, are $\{0, -1/8, -1/4, -3/8, -1/2, 1/2, 3/8, 1/4, 1/8\}$. Transmit beamspace energy P and the total number of the selected pulses within each period for $M_{\mathrm{v}} \in [9, 30]$ are calculated, and results are shown in Fig. 6. Observing this figure, transmit beamspace energy P varies with M_{v}, and does not always decrease or increase as M_{v} increases. While the number of selected pulses remains unchanged, the transmit beamspace energy P increases as M_{v} gets larger. This is because a larger M_{v} leads the selected beams to approach the center of $\mathbf{\Theta}$, resulting in more transmit energy of sidelobes distributed within $\mathbf{\Theta}$. However, as long as more pulses are added, P falls sharply, and then gradually climbs until the number of selected pulses increases again. More selected pulses lead to more energy of sidelobes and even of mainlobes dispersing out of $\mathbf{\Theta}$, which explains why P falls sharply when more beams are comprised.

The mainlobe direction $\theta_{\mathrm{b},q}$ is used as an indicator to determine which modulation pulse vectors are selected for transmit energy focusing, but the selection criterion is flexible and should be adjusted to meet other requirements. In the following example, the number of selected pulses is required to be no smaller than M_{t} in order to ensure the maximum number of detectable targets. In such a case, $M_{\mathrm{v}} = 16$ is set, and 8 instead of 9 pulses are selected as an example to compare its performance to traditional DDMA MIMO radars with $M_{\mathrm{t}} = 8$. A higher beamspace energy P can be obtained by choosing a higher M_{v} to some extent, but not always, as is shown in Fig. 6. Meanwhile, the maximum number of detectable targets of parameter estimation also influences the value of M_{v} selected. Therefore, both the beamspace energy distribution and the required number of detectable targets should be considered when selecting a proper M_{v} for slow-time TB MIMO radars.

C. Example 3: Performance Comparison of Parameter Estimation

In this example, parameter estimation performance of the proposed method is assessed in two scenarios: targets that are distantly spaced and targets that are closely spaced. The performance of the proposed method is also compared to that of three other algorithms, including ESPRIT [26], CPD [38], and PARAFAC-Direct [39]. CRBs for both PARAFAC-Direct and the proposed methods are given as well. The detailed derivation of CRBs can be found in the Appendix. According to the configuration of the proposed L-shaped array radar, one transmit subarray is arranged along z-axis, while the receive array is arranged along x-axis. Thus, transmitter matrix $\mathbf{A}_{\mathrm{z,TB}}$ is associated with elevation ϕ, while receiver matrix $\mathbf{B}$ is associated with azimuth φ. By performing the proposed method on the separated signal from the z-axis transmit subarray, $\{\phi_k\}_{k=1}^K$ using $\mathbf{A}_{\mathrm{z,TB}}$ and $\{\varphi_k\}_{k=1}^K$ using $\mathbf{B}$ can be easily paired.

Assuming that $\mathbf{\Theta}$ is known, $M_{\mathrm{v}} = 16$ and the selected pulse set is $\mathcal{I} = \{1, 2, 3, 4, 13, 14, 15, 16\}$, then the corresponding beam mainlobe directions $\{\cos\theta_{\mathrm{b},q}\}_{q\in\mathcal{I}}$ for the selected pulses are $\{0, -1/8, -1/4, -3/8, 1/2, 3/8, 1/4, 1/8\}$. The root mean square error (RMSE) and the probability of source resolution versus SNR for azimuth φ, elevation ϕ, and velocity v are evaluated. RMSE is a standard metric used to measure the estimation error, and it is defined as

$$\mathrm{RMSE} = \sqrt{\frac{1}{N}\sum_{i=1}^{N}(x - \hat{x}_i)^2} \tag{45}$$

where N is the number of observations, x represents the true value of a parameter to be estimated, and $\hat{x}_i$ is the estimate for the ith trial. $N = 300$ Monte Carlo trials are performed throughout this section. The probability of resolution will be defined later. Considering that this example focuses on parameter estimation after transmit subarray signals separation, to ensure the ideal independence of the subarrays, two orthogonal waveforms (see (46)) are used as transmit baseband waveforms in this example

$$\mathrm{u}_i(t) = \mathrm{rect}\left(\frac{t - T_{\mathrm{p}}/2}{T_{\mathrm{p}}}\right) e^{j2\pi\frac{i}{T_{\mathrm{p}}}t}, \quad i = 1, 2. \tag{46}$$

First, two distant targets are set with $\varphi = \{80^\circ, 88^\circ\}$, $\phi = \{92^\circ, 102^\circ\}$, and $\mathbf{v} = \{0.4v_{\max}, 0.6v_{\max}\}$, and their estimation results are shown in Fig. 7. The first two figures show the angle estimation results of azimuth φ using the x-subarray transmitter and elevation ϕ using z-subarray transmitter, respectively, and it can be found that they almost share the same results for each algorithm. To assess the performance of the proposed method precisely, only the related information in the estimated transmitter matrices $\mathbf{A}_{\mathrm{x,TB}}$ and $\mathbf{A}_{\mathrm{z,TB}}$ defined in (35) are utilized

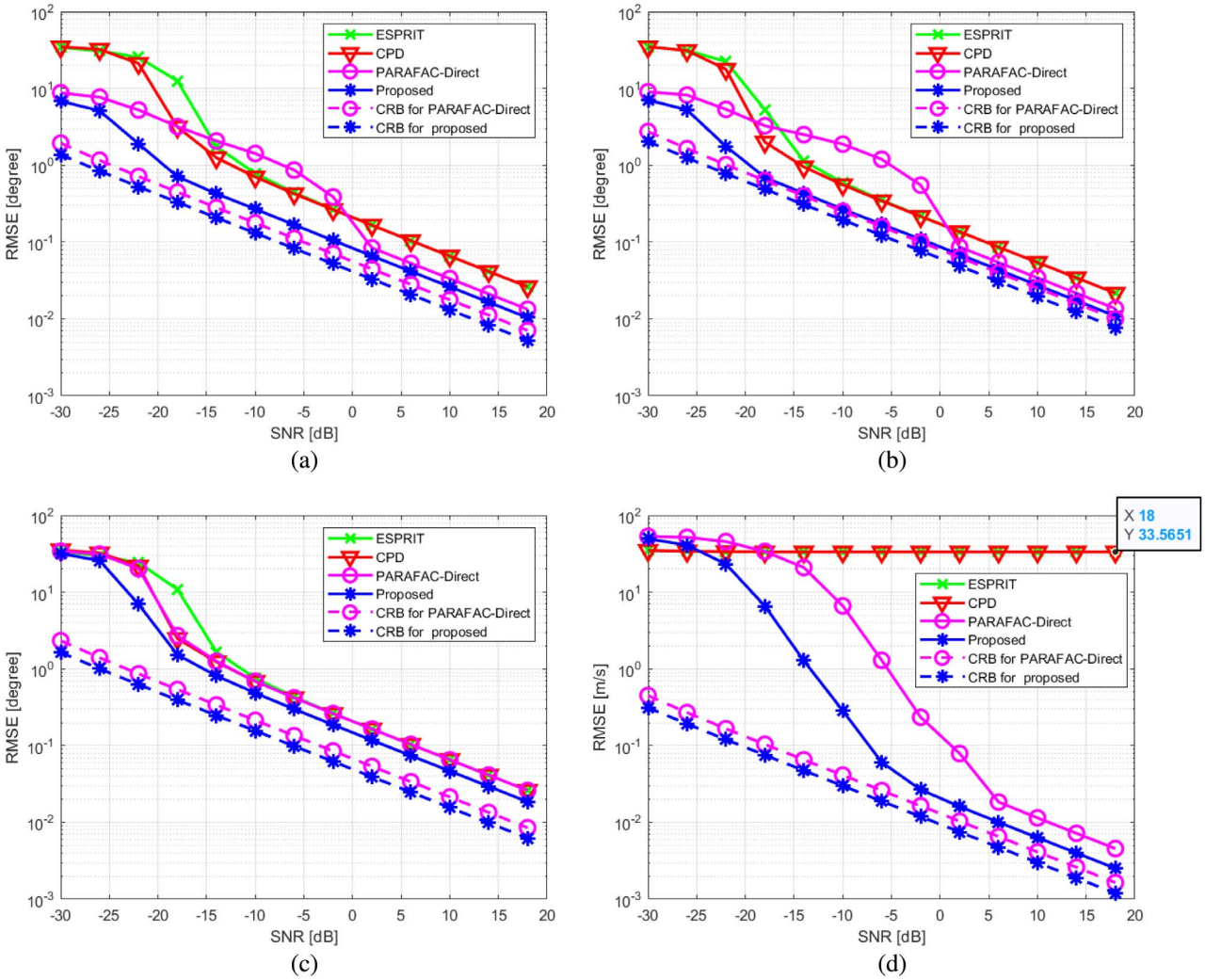

Fig. 7. RMSE results of 2 distantly spaced targets. (a) Azimuth φ by transmit x-subarray. (b) Elevation ϕ by transmit z-subarray. (c) Azimuth φ by receive array. (d) Velocity.

for angle estimation here.[6] ESPRIT and CPD achieve nearly the same performance except that CPD gains lower/better RMSE results than ESPRIT for lower SNR cases, which confirms that the multi-linear structure preserved in tensor-based signal models leads to better performance in lower SNR cases. The performance of the PARAFAC-Direct method is worse than ESPRIT and CPD when SNR is roughly in the range of -20 dB to 0 dB, while it starts to outperform them when SNR is larger than 0 dB. The proposed slow-time TB MIMO technique outperforms all aforementioned methods, particularly when SNRs are low, which is mainly attributed to the optimization of transmit energy distribution.

The results of azimuth estimation only using the receive array are shown in Fig. 7(c). They are obtained by averaging the RMSE results using the signals of x-subarray and z-subarray, which can be described as

$$\overline{\mathrm{RMSE}} = \frac{1}{2}\left(\sqrt{\frac{1}{K}\sum_{k=1}^{K}\mathrm{RMSE}_{\mathrm{x},k}^2} + \sqrt{\frac{1}{K}\sum_{k=1}^{K}\mathrm{RMSE}_{\mathrm{z},k}^2}\right) \tag{47}$$

where $\mathrm{RMSE}_{\mathrm{x},k}$ and $\mathrm{RMSE}_{\mathrm{z},k}$ are the RMSE results of the kth target for x-subarray and z-subarray, respectively. For the azimuth estimation using the receive array, ESPRIT, CPD, and PARAFAC-Direct produce comparable results, while the proposed method outperforms the other three methods tested. However, the improvement of azimuth angle estimation using the receive array is smaller than the improvement by using transmit arrays in Fig. 7(a), confirming once again that transmit energy optimization contributes to performance improvement.

To validate the proposed method's ability to resolve velocity ambiguity, the velocity of the second target is changed to $4.6v_{\max}$, while other parameters remain the same as in the previous experiment of this example. As it is illustrated in Fig. 7(d), only the results of PARAFAC-Direct and the proposed method

[6]Note that the receive array and the transmit subarray along z-axis can form a virtual URA that can also be used for DOA estimation, but to keep the focus on transmit energy focusing, the estimates based on matrices $\mathbf{A}_{\mathrm{x,TB}}$ and $\mathbf{A}_{\mathrm{z,TB}}$ are sufficient to demonstrate the benefits of the proposed approach.

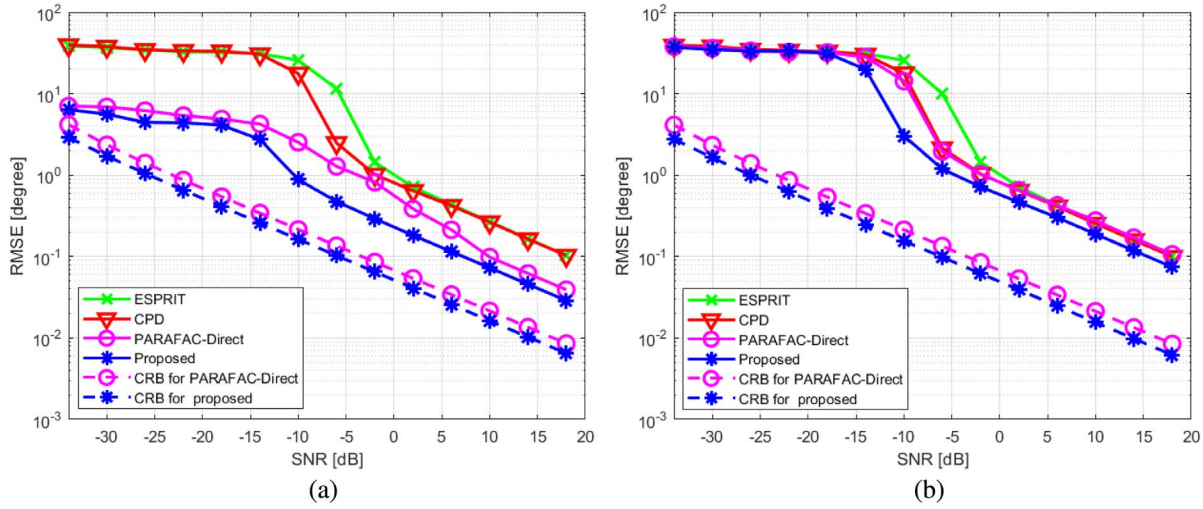

Fig. 8. RMSE results of 2 closely spaced targets. (a) Angle estimation by transmit array. (b) Azimuth φ estimation by receive array.

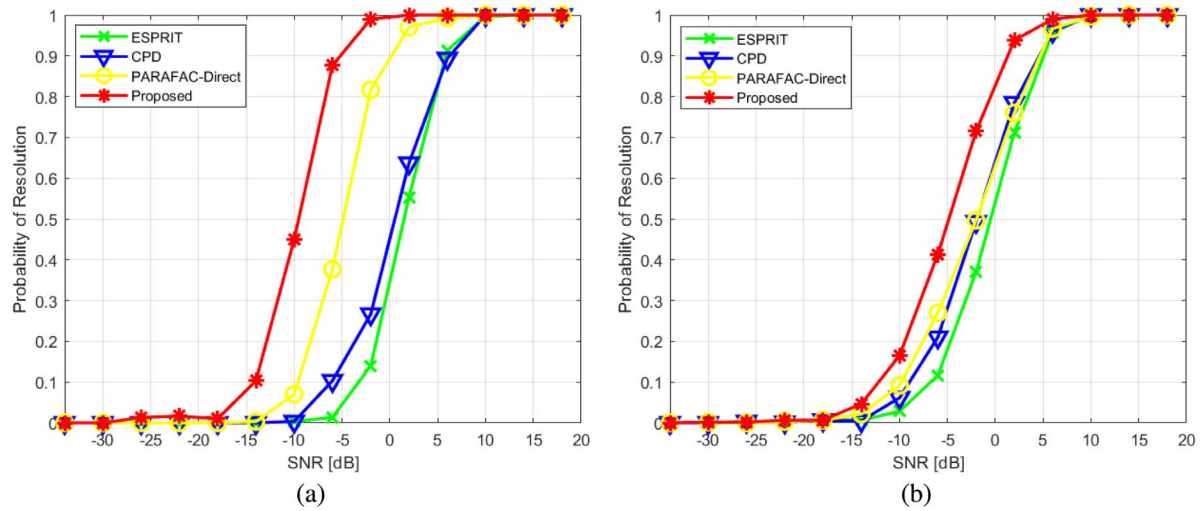

Fig. 9. Probability of target resolution versus SNR of 2 closely spaced targets. (a) Angle estimation by transmit array. (b) Azimuth φ estimation by receive array.

follow the descending trends of RMSE versus SNR, while RMSEs of ESPRIT and CPD methods are high (around $33.57\ \mathrm{m/s}$) even at high SNRs. It is because ESPRIT and CPD methods are unable to resolve velocity ambiguity. Besides the ability to resolve Doppler ambiguity, the proposed method achieves lower RMSEs than the PARAFAC-Direct method, especially for the SNRs lower than 0 dB. It is also noteworthy that Doppler ambiguity makes it difficult for DDMA-based ESPRIT and CPD methods to determine which transmit elements that the signals come from, even after signal separation, rendering these two methods invalid for DOA estimation. It demonstrates once again that the proposed method may achieve velocity disambiguation and improved performance of parameter estimation at the same time.

Next, to assess the angle resolution of the proposed method, two closely-spaced targets with $\varphi = \{86°, 88°\}$, $\phi = \{100°, 102°\}$, and $\mathbf{v} = \{0.4v_{\max}, 0.6v_{\max}\}$ are used in the following experiment. Given that the estimation results of φ and ϕ are similar as illustrated in Fig. 7(a) and 7(b), the angle estimation results given in Fig. 8(a) are obtained by averaging the results of φ and ϕ using two transmit matrices, and its calculation method can refer to (47). The RMSE results for azimuth angles estimated by receive array are shown in Fig. 8(b). Similar to the previous experiment, the proposed method outperforms the other three methods, especially for the estimation results using transmit array in Fig. 8(a).

The probability of target resolution, which refers to the likelihood that an algorithm can resolve two closely spaced targets, is assessed among four methods. Two targets are considered to be resolved if the angle estimation error satisfies

$$|\hat{\theta} - \theta| < \frac{\Delta\theta}{2} \tag{48}$$

where $\hat{\theta}$ and θ are the estimated and real angle values, respectively, and $\Delta\theta = |\theta_1 - \theta_2|$ is the absolute angle difference between two targets. The angle resolution results by transmit and receive array are shown in Fig. 9(a) and 9(b), respectively. Transmit matrices can be used to determine azimuth φ and

elevation ϕ. To locate source targets in 3-D geometry, two closely-spaced targets are considered to be resolved if their azimuth φ and elevation ϕ fulfill (48) simultaneously. Thus, only when φ and ϕ are resolvable simultaneously, the result is recognized as resolvable in Fig. 9(a). Observing Fig. 9, the probability of target resolution starts ramping up for each method tested as SNR value increases until it eventually reaches 100% correct resolution, and the SNR value at which this transition happens is called as SNR threshold [40]. It can be clearly seen from Fig. 9(a) that transitions of ESPRIT, CPD, and PARAFAC-Direct techniques happen at nearly the same SNR value, while the SNR threshold of the proposed method is around 10–15 dB lower than the other three methods tested. When compared to angle estimation by the transmit array, the proposed method also outperforms all other methods in angle estimation by the receive array, as is depicted in Fig. 9(b), but its improvement is less evident, same as in the scenario with targets placed significantly apart from one another.

From two experiments conducted in this example, it can be found that the proposed method achieves an evident performance improvement of parameter estimation compared to ESPRIT, CPD, and PARAFAC-Direct in terms of both estimation accuracy and closely spaced targets resolution.

VI. Conclusion

In this paper, a technique called slow-time TB MIMO for L-shaped array radar is proposed to improve parameter estimation performance and resolve velocity ambiguity. A new phase modulation matrix for slow-time TB MIMO radar is designed to achieve transmit energy optimization. By dividing the entire spectrum into more subbands than the number of transmit antenna elements, adjacent beams formed by pulse vectors get closer, and more transmit beams can be comprised within the region of interest. The new modulation matrix for the proposed slow-time TB MIMO radar is constructed from those pulse vectors whose beams are directed toward the desired region. A new tensor-based signal model is designed for parameter estimation, which preserves the multi-linear structure of signal measurements. Moreover, it also preserves the velocity information for velocity disambiguation which is missing in the matrix-based methods with Doppler spectrum division. The parameter estimation performance of the proposed method is enhanced, especially for lower SNR cases, and velocity ambiguity is alleviated. Simulation results have verified that the proposed slow-time TB MIMO radar technique has more effective parameter estimation performance than the other existing methods.

Appendix
CRBs Derivation

First, the CRBs are derived for the signal of z-subarray. Vectorizing $\mathbf{Y}_{\mathrm{z}}$ in (31) into $\mathbf{y}_{\mathrm{z}} = \mathrm{vec}(\mathbf{Y}_{\mathrm{z}}) \in \mathbb{C}^{QM_{\mathrm{r}} \times 1}$, the received signal can be re-expressed as

$$\mathbf{y}_{\mathrm{z}} = \sum_{k=1}^{K} \sigma_k \mathbf{b}(\varphi_k) \odot \left[\mathbf{W}_{\mathrm{z,TB}}^{T} \mathbf{a}_{\mathrm{z}}(\phi_k) * \mathbf{d}(f_k)\right] + \mathrm{vec}(\mathbf{Z}_{\mathrm{z}}) \tag{49}$$

where $\mathrm{vec}(\cdot)$ denotes the vectorization operation. Given that the receive array is set as a ULA along the x-axis in the simulation experiments, $\mathbf{b}(\varphi_k)$ is used here. The corresponding covariance matrix is then

$$\mathbf{R} = \mathbf{y}_{\mathrm{z}} \mathbf{y}_{\mathrm{z}}^{H} = \mathbf{C}\mathbf{P}\mathbf{C}^{H} + \sigma_{\mathrm{n}}^{2}\mathbf{I} \tag{50}$$

where $\mathbf{P}$ is a diagonal matrix with diagonal elements $\sigma_1^2, \sigma_2^2, \ldots, \sigma_K^2, \sigma_{\mathrm{n}}^2$ is the noise variance, $\mathbf{I}$ is an identity matrix of size $QM_{\mathrm{r}} \times QM_{\mathrm{r}}$, and the kth column of $\mathbf{C}$ is given as

$$\mathbf{c}_k = \mathbf{b}(\varphi_k) \odot \left[\mathbf{W}_{\mathrm{z,TB}}^{T} \mathbf{a}_{\mathrm{z}}(\phi_k) * \mathbf{d}(f_k)\right]. \tag{51}$$

Denote the unknown parameter vector as

$$\boldsymbol{\rho} = [\varphi_1, \ldots, \varphi_K, \phi_1, \ldots, \phi_K, f_1, \ldots, f_K, \sigma_1^2, \ldots, \sigma_K^2, \sigma_{\mathrm{n}}^2]^{T}. \tag{52}$$

According to (4) in [46] the (m, n)-th element of the Fisher information matrix (FIM) can be found as

$$[\mathbf{FIM}_{\mathrm{z}}]_{m,n} = N_{\mathrm{s}} \mathrm{Tr}\left(\frac{\partial \mathbf{R}}{\partial \rho_m} \mathbf{R}^{-1} \frac{\partial \mathbf{R}}{\partial \rho_n} \mathbf{R}^{-1}\right) \quad m, n = 1, 2, \ldots, 4K+1 \tag{53}$$

where $\mathrm{Tr}(\cdot)$ denotes the trace of a matrix, ρ_n is the nth element of $\boldsymbol{\rho}$, $\partial \mathbf{R}/\partial \rho_n$ stands for the partial derivative of $\mathbf{R}$ with respect to ρ_n, $(\cdot)^{-1}$ denotes the inverse of a matrix, and N_{s} is the number of snapshots. In the simulation experiments, $N_{\mathrm{s}} = 1$, i.e., a single snapshot is used.

The partial derivatives of $\mathbf{R}$ with respect to $\{\varphi_k\}_{k=1}^{K}$, $\{\phi_k\}_{k=1}^{K}$, $\{f_k\}_{k=1}^{K}$, $\{\sigma_k^2\}_{k=1}^{K}$, and σ_{n}^2 in the case of z-subarray can be calculated by

$$\begin{aligned}
\frac{\partial \mathbf{R}}{\partial \varphi_k} &= \sigma_k^2 \left(\frac{\partial \mathbf{c}_k}{\partial \varphi_k} \mathbf{c}_k^{H} + \mathbf{c}_k \frac{\partial \mathbf{c}_k^{H}}{\partial \varphi_k}\right) \\
\frac{\partial \mathbf{c}_k}{\partial \varphi_k} &= \frac{\partial \mathbf{b}(\varphi_k)}{\partial \varphi_k} \odot \left[\mathbf{W}_{\mathrm{z,TB}}^{T} \mathbf{a}_{\mathrm{z}}(\phi_k) * \mathbf{d}(f_k)\right] \\
\frac{\partial \mathbf{R}}{\partial \phi_k} &= \sigma_k^2 \left(\frac{\partial \mathbf{c}_k}{\partial \phi_k} \mathbf{c}_k^{H} + \mathbf{c}_k \frac{\partial \mathbf{c}_k^{H}}{\partial \phi_k}\right) \\
\frac{\partial \mathbf{c}_k}{\partial \phi_k} &= \mathbf{b}(\varphi_k) \odot \left[\mathbf{W}_{\mathrm{z,TB}}^{T} \frac{\partial \mathbf{a}_{\mathrm{z}}(\phi_k)}{\partial \phi_k} * \mathbf{d}(f_k)\right] \\
\frac{\partial \mathbf{R}}{\partial f_k} &= \sigma_k^2 \left(\frac{\partial \mathbf{c}_k}{\partial f_k} \mathbf{c}_k^{H} + \mathbf{c}_k \frac{\partial \mathbf{c}_k^{H}}{\partial f_k}\right) \\
\frac{\partial \mathbf{c}_k}{\partial f_k} &= \mathbf{b}(\varphi_k) \odot \left[\mathbf{W}_{\mathrm{z,TB}}^{T} \mathbf{a}_{\mathrm{z}}(\phi_k) * \frac{\partial \mathbf{d}(f_k)}{\partial f_k}\right] \\
\frac{\partial \mathbf{R}}{\partial \sigma_k^2} &= \mathbf{c}_k \mathbf{c}_k^{H}, \quad \frac{\partial \mathbf{R}}{\partial \sigma_{\mathrm{n}}^2} = \mathbf{I}.
\end{aligned} \tag{54}$$

Using (53), FIM for the signal of z-subarray can be obtained, and CRBs for azimuth φ, elevation ϕ, and Doppler shift f can be respectively computed as

$$\varphi_{\mathrm{CRB}} = \sqrt{\frac{1}{K} \sum_{i=1}^{K} \left[\mathbf{FIM}_{\mathrm{z}}^{-1}\right]_{i,i}}$$

$$\phi_{\mathrm{CRB}} = \sqrt{\frac{1}{K}\sum_{i=K+1}^{2K}\left[\mathbf{FIM}_{\mathrm{z}}{}^{-1}\right]_{i,i}}$$
$$f_{\mathrm{CRB}} = \sqrt{\frac{1}{K}\sum_{i=2K+1}^{3K}\left[\mathbf{FIM}_{\mathrm{z}}{}^{-1}\right]_{i,i}}. \tag{55}$$

The CRBs for the case of x-subarray can be derived in a similar manner. Considering that there is no information about $\{\phi_k\}_{k=1}^{K}$ contained in the signal transmitted from x-subarray, the unknown parameter vector becomes

$$\boldsymbol{\rho} = [\varphi_1, \ldots, \varphi_K, f_1, \ldots, f_K, \sigma_1^2, \ldots, \sigma_K^2, \sigma_{\mathrm{n}}^2]^T. \tag{56}$$

The derivative of $\mathbf{c}_k$ with respect to φ_k in this case becomes

$$\frac{\partial \mathbf{c}_k}{\partial \varphi_k} = \frac{\partial \mathbf{b}(\varphi_k)}{\partial \varphi_k} \odot \left[\mathbf{W}_{\mathrm{x,TB}}^T \mathbf{a}_{\mathrm{x}}(\varphi_k) * \mathbf{d}(f_k)\right] + \mathbf{b}(\varphi_k) \odot \left[\mathbf{W}_{\mathrm{x,TB}}^T \frac{\partial \mathbf{a}_{\mathrm{x}}(\varphi_k)}{\partial \varphi_k} * \mathbf{d}(f_k)\right]. \tag{57}$$

The corresponding CRBs of φ and f can be calculated by

$$\varphi_{\mathrm{CRB}} = \sqrt{\frac{1}{K}\sum_{i=1}^{K}\left[\mathbf{FIM}_{\mathrm{x}}{}^{-1}\right]_{i,i}}$$
$$f_{\mathrm{CRB}} = \sqrt{\frac{1}{K}\sum_{i=K+1}^{2K}\left[\mathbf{FIM}_{\mathrm{x}}{}^{-1}\right]_{i,i}} \tag{58}$$

where $\mathbf{FIM}_{\mathrm{x}}$ is the FIM for the signal of x-subarray.

The FIMs for the PARAFAC-Direct model have the same form, and the only difference is that matrices $\mathbf{W}_{\mathrm{x,TB}}$ and $\mathbf{W}_{\mathrm{z,TB}}$ are substituted by $\mathbf{W}_{\mathrm{x}}$ and $\mathbf{W}_{\mathrm{z}}$, respectively.

REFERENCES

[1] E. Fishler, A. Haimovich, R. Blum, D. Chizhik, L. Cimini, and R. Valenzuela, "MIMO radar: An idea whose time has come," in *Proc. IEEE Radar Conf.*, Philadelphia, PA, USA, 2004, pp. 71–78.

[2] J. Li and P. Stoica, "MIMO radar with colocated antennas," *IEEE Signal Process. Mag.*, vol. 24, no. 5, pp. 106–114, Sep. 2007.

[3] N. H. Lehmann et al., "Evaluation of transmit diversity in MIMO-radar direction finding," *IEEE Trans. Signal Process.*, vol. 55, no. 5, pp. 2215–2225, May 2007.

[4] F. Daum and J. Huang, "MIMO radar: Snake oil or good idea?" *IEEE Aerosp. Electron. Syst. Mag.*, vol. 24, no. 5, pp. 8–12, May 2009.

[5] A. M. Haimovich, R. S. Blum, and L. J. Cimini, "MIMO radar with widely separated antennas," *IEEE Signal Process. Mag.*, vol. 25, no. 1, pp. 116–129, Dec. 2007.

[6] R. J. Mailloux, "Phased array theory and technology," *Proc. IEEE*, vol. 70, no. 3, pp. 246–291, Mar. 1982.

[7] A. Hassanien and S. A. Vorobyov, "Phased-MIMO radar: A tradeoff between phased-array and MIMO radars," *IEEE Trans. Signal Process.*, vol. 58, no. 6, pp. 3137–3151, Jun. 2010.

[8] H. Sun, F. Briguiand, and M. Lesturgie, "Analysis and comparison of MIMO radar waveforms," in *Proc. IEEE Int. Radar Conf.*, Oct. 2014, pp. 1–6.

[9] W. van Rossum and L. Anitori, "Doppler ambiguity resolution using random slow-time code division multiple access MIMO radar with sparse signal processing," in *Proc. IEEE Radar Conf.*, Oklahoma City, OK, USA, 2018, pp. 441–446.

[10] C. M. Schmid, R. Feger, C. Pfeffer, and A. Stelzer, "Motion compensation and efficient array design for TDMA FMCW MIMO radar systems," in *Proc. 6th Eur. Conf. Antennas Propag. (EUCAP)*, Prague, Czech Republic, 2012, pp. 1746–1750.

[11] F. G. Jansen, "Automotive radar Doppler division MIMO with velocity ambiguity resolving capabilities," in *Proc. 16th European Radar Conf. (EuRAD)*, Paris, France, 2019, pp. 245–248.

[12] L. Ren et al., "Short-time state-space method for micro-Doppler identification of walking subject using UWB impulse Doppler radar," *IEEE Trans. Microw. Theory Techn.*, vol. 66, no. 7, pp. 3521–3534, May 2018.

[13] R. Yadav, P. K. Dahiya, and R. Mishra, "A high performance 76.5 GHz FMCW RADAR for advanced driving assistance system," in *Proc. 3rd Int. Conf. Signal Process. Integr. Netw. (SPIN)*, Noida, India, Feb. 2016, pp. 383–388.

[14] K. F. Chang et al., "77-GHz automotive radar sensor system with antenna integrated package," *IEEE Trans. Compon. Packag. Manuf. Technol.*, vol. 4, no. 2, pp. 352–359, Feb. 2014.

[15] Y. Hua, T. K. Sarkar, and D. Weiner, "An L-shaped array for estimating 2-D directions of wave arrival," *IEEE Trans. Antennas Propag.*, vol. 39, no. 2, pp. 143–146, Feb. 1991.

[16] J. F. Gu, W. P. Zhu, and M. N. S. Swamy, "Joint 2-D DOA estimation via sparse L-shaped array," *IEEE Trans. Signal Process.*, vol. 63, no. 5, pp. 1171–1182, Mar. 2015.

[17] N. Tayem and H. M. Kwon, "L-shape 2-dimensional arrival angle estimation with propagator method," *IEEE Trans. Antennas Propag.*, vol. 53, no. 5, pp. 1622–1630, May 2005.

[18] J. F. del Rio and M. F. Catedra-Perez, "The matrix pencil method for two-dimensional direction of arrival estimation employing an L-shaped array," *IEEE Trans. Antennas Propag.*, vol. 45, no. 11, pp. 1693–1694, Nov. 1997.

[19] Y. Wu, G. Liao, and H. C. So, "A fast algorithm for 2-D direction-of-arrival estimation," *Signal Process.*, vol. 83, no. 8, pp. 1827–1831, Aug. 2003.

[20] X. Wu and W. Zhu, "On efficient gridless methods for 2-D DOA estimation with uniform and sparse L-shaped arrays" *Signal Process.*, vol. 191, no. 2, Feb. 2022, Art. no. 108351.

[21] Y. Dong, C. Dong, W. Liu, H. Chen, and G. Zhao, "On efficient gridless methods for 2-D DOA estimation with uniform and sparse L-shaped arrays," *IEEE Trans. Signal Process.*, vol. 65, no. 4, pp. 495–499, Apr. 2017.

[22] F. Xu, H. Zheng, and S. A. Vorobyov, "Tensor-based 2D DOA estimation for L-shaped nested array," *IEEE Trans. Aerosp. Electron. Syst.*, vol. 60, no. 1, pp. 604–618, Feb. 2024.

[23] H. Krim and M. Viberg, "Two decades of array signal processing research: The parametric approach," *IEEE Signal Process. Mag.*, vol. 13, no. 4, pp. 67–94, Jul. 1996.

[24] A. Barabell, "Improving the resolution performance of eigenstructure-based direction-finding algorithms," in *Proc. IEEE Int. Conf. Acoust., Speech, Signal Process.*, Boston, MA, USA, vol. 8, 1983, pp. 336–339.

[25] R. Schmidt, "Multiple emitter location and signal parameter estimation," *IEEE Trans. Antennas Propag.*, vol. 34, no. 3, pp. 276–280, Mar. 1986.

[26] J. Chen, H. Gu, and W. Su, "Angle estimation using ESPRIT without pairing in MIMO radar," *Electron. Lett.*, vol. 44, no. 24, pp. 1422–1423, Nov. 2008.

[27] H. Chen, F. Ahmad, S. A. Vorobyov, and F. Porikli, "Tensor decompositions in wireless communications and MIMO radar," *IEEE J. Sel. Topics Signal Process.*, vol. 15, no. 3, pp. 438–453, Apr. 2021.

[28] M. Cao, S. A. Vorobyov, and A. Hassanien, "Transmit array interpolation for DOA estimation via tensor decomposition in 2-D MIMO radar," *IEEE Trans. Signal Process.*, vol. 65, no. 19, pp. 5225–5239, Oct. 2017.

[29] M. Haardt, F. Roemer, and G. Del Galdo, "Higher-order SVD-based subspace estimation to improve the parameter estimation accuracy in multidimensional harmonic retrieval problems," *IEEE Trans. Signal Process.*, vol. 56, no. 7, pp. 3198–3213, Jul. 2008.

[30] W. Sun, H. C. So, F. K. W. Chan, and L. Huang, "Tensor approach for eigenvector-based multi-dimensional harmonic retrieval," *IEEE Trans. Signal Process.*, vol. 61, no. 13, pp. 3378–3388, Jul. 2013.

[31] L. D. Lathauwer, B. D. Moor, and J. Vandewalle, "A multilinear singular value decomposition," *SIAM J. Matrix Anal. Appl.*, vol. 21, no. 4, pp. 1253–1278, 2000.

[32] D. Nion and N. D. Sidiropoulos, "Tensor algebra and multidimensional harmonic retrieval in signal processing for MIMO radar," *IEEE Trans. Signal Process.*, vol. 58, no. 11, pp. 5693–5705, Nov. 2010.

[33] T. G. Kolda and B. W. Bader, "Tensor decompositions and applications," *SIAM Rev.*, vol. 51. no. 3, pp. 455–500, Aug. 2009.

[34] A. L. F. de Almeida, G. Favier, and J. C. M. Mota, "Constrained tensor modeling approach to blind multiple-antenna CDMA schemes," *IEEE Trans. Signal Process.*, vol. 56, no. 6, pp. 2417–2428, Jun. 2008.

[35] F. Xu, M. W. Morency, and S. A. Vorobyov, "DOA estimation for transmit beamspace MIMO radar via tensor decomposition with Vandermonde factor matrix," *IEEE Trans. Signal Process.*, vol. 70, pp. 2901–2917, 2022.
[36] H. Zheng, C. Zhou, S. A. Voroboyv, Q. Wang, and Z. Shi, "Decomposed CNN for sub-Nyquist tensor-based 2-D DOA estimation," *IEEE Signal Process. Lett.*, vol. 30, pp. 708–712, 2023.
[37] H. Zheng, C. Zhou, S. A. Vorobyov, and Z. Shi, "Tensorized neural layer decomposition for 2D DOA estimation," in *Proc. 48th IEEE Int. Conf. Acoust., Speech, Signal Process.*, Rhodes Island, Greece, Jun. 2023, pp. 1–5.
[38] F. Xu, S. A. Vorobyov, and X. Yang, "Joint DOD and DOA estimation in slow-time MIMO radar via PARAFAC decomposition," *IEEE Signal Process. Lett.*, vol. 27, pp. 1495–1499, 2020.
[39] L. Wang, B. Li, C. Yu, A. Liu, and X. Ji, "PARAFAC-Direct: A joint parameters estimation method for slow-time MIMO," *IEEE Signal Process. Lett.*, vol. 29, pp. 732–736, 2022.
[40] A. Hassanien and S. A. Vorobyov, "Transmit energy focusing for DOA estimation in MIMO radar with colocated antennas," *IEEE Trans. Signal Process.*, vol. 59, no. 6, pp. 2669–2682, Jun. 2011.
[41] T. Zhang, F. Xu, and S. A. Vorobyov, "Transmit energy focusing for parameter estimation in transmit beamspace slow-time MIMO radar," in *Proc. IEEE Int. Conf. Acoust., Speech, Signal Process.*, Rhodes Island, Greece, Jun. 2023, pp. 1–5.
[42] F. Xu, S. A. Vorobyov, and F. Yang, "Transmit beamspace DDMA based automotive MIMO radar," *IEEE Trans. Veh. Technol.*, vol. 71, no. 2, pp. 1669–1684, Feb. 2022.
[43] P. Swerling, "Probability of detection for fluctuating targets," *IRE Trans. Inf. Theory*, vol. 6, no. 2, pp. 269–308, Apr. 1960.
[44] J. O. Smith, "Introduction to digital filters with audio applications," Stanford, CA, USA: Stanford University, 2007.
[45] N. D. Sidiropoulos, R. Bro, and G. B. Giannakis, "Parallel factor analysis in sensor array processing," *IEEE Trans. Signal Process.*, vol. 48, no. 8, pp. 2377–2388, Aug. 2000.
[46] P. Stoica, E. G. Larsson, and A. B. Gershman, "The stochastic CRB for array processing: A textbook derivation," *IEEE Signal Process. Lett.*, vol. 8, no. 5, pp. 148–150, May 2001.

Tingting Zhang (Student Member, IEEE) received the M.Eng. degree in electronic engineering from Nanjing University of Science and Technology, Nanjing, China, in 2023. She is currently working toward the Ph.D. degree with the Department of Information and Communications Engineering, Aalto University, Finland. Her research interests include multiple-input multiple-output radar transmit energy optimization and direction-of-arrival estimation.

Sergiy A. Vorobyov (Fellow, IEEE) received the M.Sc. and Ph.D. degrees in systems and control from the National University of Radio Electronics, Kharkiv, Ukraine, in 1994 and 1997, respectively. He is a Professor with the Department of Information and Communications Engineering, Aalto University, Finland. Since his graduation, he held various faculty and research positions with the University of Alberta, Canada; the Joint Research Institute between Heriot-Watt University and Edinburgh University, U.K.; Duisburg-Essen University and Darmstadt University of Technology, Germany; McMaster University, Canada; the Institute of Physical and Chemical Research, Japan; and the National University of Radio Electronics, Ukraine. His research interests include optimization and multiliner algebra methods in signal processing and data analysis; statistical, array, and graph signal processing; estimation, detection, and learning theory and methods; computational imaging; and multiantenna, very large, cooperative, and cognitive systems. He was the recipient of the 2004 IEEE Signal Processing Society Best Paper Award, the 2007 Alberta Ingenuity New Faculty Award, the 2011 Carl Zeiss Award (Germany), the 2012 NSERC Discovery Accelerator Award, IEEE ICASSP 2023 Top 3% paper recognition, and other awards. He was a Senior Area Editor for IEEE SIGNAL PROCESSING LETTERS from 2016 to 2020, and an Associate Editor for IEEE TRANSACTIONS ON SIGNAL PROCESSING from 2006 to 2010 and IEEE SIGNAL PROCESSING LETTERS from 2007 to 2009. He was a member of the Sensor Array and Multi-Channel Signal Processing and Signal Processing for Communications and Networking Technical Committees of the IEEE Signal Processing Society from 2007 to 2012 and 2010 to 2016, respectively. He was the Track Chair for Asilomar 2011, Pacific Grove, CA, USA; a Technical Co-Chair for IEEE CAMSAP 2011, Puerto Rico; the Tutorial Chair for ISWCS 2013, Ilmenau, Germany; a Technical Co-Chair for IEEE SAM 2018, Sheffield, U.K.; a Technical Co-Chair for IEEE CAMSAP 2023, Costa Rica; and a General Co-Chair for EUSIPCO 2023, Helsinki, Finland.

Feng Xu (Member, IEEE) received the Ph.D. degree in information and communication engineering from the School of Information and Electronics, Beijing Institute of Technology, Beijing, China, in 2021. From 2019 to 2021, he was a Visiting Doctoral Student with the Department of Signal Processing and Acoustics, Aalto University, Espoo, Finland, where he is currently a Research Assistant. His research interests include array signal processing, radar, communication, and tensor decomposition.